J. Fluid Mech. (2013), *vol.* 726, *pp.* 624–655.
doi:10.1017/jfm.2013.223

Lock-in and quasiperiodicity in a forced hydrodynamically self-excited jet

Larry K. B. Li† and Matthew P. Juniper

Department of Engineering, University of Cambridge, Trumpington Street, Cambridge CB2 1PZ, UK

(Received 13 September 2012; revised 3 April 2013; accepted 25 April 2013;
first published online 11 June 2013)

The ability of hydrodynamically self-excited jets to lock into strong external forcing is well known. Their dynamics before lock-in and the specific bifurcations through which they lock in, however, are less well known. In this experimental study, we acoustically force a low-density jet around its natural global frequency. We examine its response leading up to lock-in and compare this to that of a forced van der Pol oscillator. We find that, when forced at increasing amplitudes, the jet undergoes a sequence of two nonlinear transitions: (i) from periodicity to $\mathbb{T}^2$ quasiperiodicity via a torus-birth bifurcation; and then (ii) from $\mathbb{T}^2$ quasiperiodicity to 1:1 lock-in via either a saddle-node bifurcation with frequency pulling, if the forcing and natural frequencies are close together, or a torus-death bifurcation without frequency pulling, but with a gradual suppression of the natural mode, if the two frequencies are far apart. We also find that the jet locks in most readily when forced close to its natural frequency, but that the details contain two asymmetries: the jet (i) locks in more readily and (ii) oscillates more strongly when it is forced below its natural frequency than when it is forced above it. Except for the second asymmetry, all of these transitions, bifurcations and dynamics are accurately reproduced by the forced van der Pol oscillator. This shows that this complex (infinite-dimensional) forced self-excited jet can be modelled reasonably well as a simple (three-dimensional) forced self-excited oscillator. This result adds to the growing evidence that open self-excited flows behave essentially like low-dimensional nonlinear dynamical systems. It also strengthens the universality of such flows, raising the possibility that more of them, including some industrially relevant flames, can be similarly modelled.

Key words: absolute/convective instability, flow control, nonlinear dynamical systems

1. Introduction

In open hydrodynamic systems, the presence of local absolute instability can give rise to global self-excited oscillations at discrete natural frequencies. If these oscillating systems are forced strongly at other frequencies, however, they can lock into the forcing and oscillate at its frequency instead, leaving no sign of the original natural mode in the power spectral density (PSD). This nonlinear adjustment process is known as synchronization, and the resulting synchronous state is known as lock-in (or phase locking; Balanov *et al.* 2009). Lock-in has been observed in various forced

† Email address for correspondence: l.li@gatescambridge.org

self-excited flows, such as cylinder wakes (Koopmann 1967; Stansby 1976; Provansal, Mathis & Boyer 1987), capillary jets (Olinger 1992), low-density jets (Sreenivasan, Raghu & Kyle 1989; Hallberg & Strykowski 2008), low-density and equidensity cross-flowing jets (Davitian *et al.* 2010; Getsinger, Hendrickson & Karagozian 2012) and jet diffusion flames (Li & Juniper 2013).

Self-excited flows were previously thought to be insensitive to external forcing before lock-in (see the review by Huerre & Monkewitz 1990), but more recent research has shown that they oscillate quasiperiodically instead. In power spectra, quasiperiodicity can be identified by sharp peaks at linear combinations of the forcing and natural frequencies (e.g. $2f_f - f_n$), but only if these frequencies are incommensurate and only if the forcing amplitude is insufficient to cause complete lock-in. This coexistence of multiple spectral components implies that quasiperiodicity is a superposition of multiple periodic motions, each at a slightly different fundamental frequency. However, because the two main frequencies are incommensurate, the system oscillates with a period of infinity and therefore never returns to exactly the same state, although it can get arbitrarily close. In other words, a quasiperiodic oscillation is recurrent but not repetitive.

Like lock-in, quasiperiodicity has been observed in various forced self-excited flows, such as cylinder wakes (Van Atta & Gharib 1987; Karniadakis & Triantafyllou 1989), capillary jets (Olinger 1992), low-density jets (Juniper, Li & Nichols 2009), low-density and equidensity cross-flowing jets (Davitian *et al.* 2010; Getsinger *et al.* 2012) and jet diffusion flames (Li & Juniper 2013). Among these, cylinder wakes have received the most attention, forming the basis for much of the existing knowledge on the nonlinear dynamics of forced hydrodynamic oscillators. In a typical study, a supercritical wake is forced, either acoustically or mechanically, around its natural frequency, and its response is examined: (i) when unforced, it oscillates periodically in a limit cycle; (ii) when forced weakly, it oscillates quasiperiodically and, if the forcing frequency is close to the natural frequency, the latter can shift towards the former (Blevins 1985; Barbi *et al.* 1986); (iii) when forced strongly, it locks into the forcing, but the minimum forcing amplitude required for this is not necessarily symmetric about the natural frequency (Blevins 1985; Provansal *et al.* 1987). Although these dynamics are well established in cylinder wakes, they are still being explored in other self-excited flows. To date, several researchers have confirmed the universal existence of quasiperiodicity and lock-in (Olinger 1993; Manneville 2010). However, few have examined these nonlinear states in detail, particularly near their transition. Hence, no one has identified the specific bifurcations through which hydrodynamic oscillators lock into external forcing.

Lock-in is expected to occur via a sequence of bifurcations as the forcing amplitude increases. This concept of transitioning between discrete nonlinear states has prompted suggestions, notably from Huerre & Monkewitz (1990), that self-excited flows can be adequately described with only a few degrees of freedom (DOFs) and can therefore be modelled as low-dimensional dynamical systems. In cylinder wakes, for example, Provansal *et al.* (1987) and Olinger (1993) showed that a forced Landau–Stuart model can accurately reproduce many features of quasiperiodicity and lock-in, including the latter's occurrence above a critical forcing amplitude and a linear increase in this amplitude with frequency detuning. However, when used to interpret experimental data, this particular model has two limitations: (i) its bifurcations to lock-in have not been rigourously analysed before, which means that, even if similarities arise, they cannot be linked to any of the universal bifurcations found in simple dynamical systems; and (ii) its validity is restricted to conditions for which the time scale of its oscillations

is much smaller than the time scale of its amplitude growth, which means that the model is valid only near the onset of global instability (i.e. near the supercritical Hopf bifurcation to the initial limit cycle) because there the saturated amplitude is still small and the waveform is still harmonic (i.e. weakly nonlinear). For the study of supercritical flows that are not necessarily close to critical, a better approach is to use a fully nonlinear model whose bifurcations to lock-in have already been well analysed. One of the simplest is the van der Pol (VDP) oscillator, a second-order ordinary differential equation whose complete set of bifurcations was analysed by Holmes & Rand (1978) and Balanov *et al.* (2009), among others. This oscillator has been used before to model various physical and biological systems (e.g. triode circuits, tectonic plates and cardiac muscles), but its use in hydrodynamics has been limited to closed flows (e.g. Rayleigh–Bénard convection; Fauve 1998) and open wake flows (Gaster 1969; Noack, Ohle & Eckelmann 1991; Baek & Sung 2000; Facchinetti, de Langre & Biolley 2002), including vortex-induced vibration (Hartlen & Currie 1970; Iwan & Blevins 1974; Facchinetti, de Langre & Biolley 2004). To our knowledge, the VDP oscillator has never been used to model open jet flows. If this can be done successfully, it would strengthen the universality of open self-excited flows and help identify the specific bifurcations through which they lock into external forcing.

In this paper, we study the nonlinear dynamics of a hydrodynamically self-excited jet in the stages near lock-in. We do this experimentally, by applying open-loop time-periodic acoustic forcing to a low-density jet: a canonical flow that is known to oscillate at a well-defined natural frequency (Monkewitz *et al.* 1990). We apply the forcing around this frequency, at varying amplitudes, and measure the response in the wavemaker region. By analysing the data within a dynamical systems framework, we discover much richer behaviour than that which is reported in the literature. We then show that this behaviour can be qualitatively reproduced with a forced VDP oscillator and use this analogy to improve our interpretation of the underlying jet dynamics, particularly to identify the specific bifurcations that cause lock-in. As well as providing new insight into the way acoustic oscillations interact with hydrodynamic oscillations, this paper shows that this complex (infinite-dimensional) forced self-excited jet can be modelled as a simple (three-dimensional) forced self-excited oscillator.

2. Methodology

2.1. *Experimental details*

The jet that we consider is axisymmetric, unconfined and non-swirling. In the absence of significant buoyancy and compressibility effects, its onset of global instability has been shown by Hallberg & Strykowski (2006) to depend on three independent parameters: (i) the density ratio between the jet and its surroundings, $S \equiv \rho_j/\rho_\infty$; (ii) the momentum thickness of the initial shear layer, θ, which is often expressed in inverse non-dimensional form as the transverse curvature, d/θ; and (iii) the jet Reynolds number, $Re \equiv \rho_j U_j d/\mu_j$, where U_j is the time-averaged bulk velocity, d is the nozzle exit diameter and μ_j is the dynamic viscosity of the jet fluid. The onset of global instability also depends on the shape and alignment of the density and velocity profiles (particularly the relative position of their inflexion points), although Srinivasan, Hallberg & Strykowski (2010) have shown that this dependence is of secondary importance if the shear layer is moderately thin ($d/\theta \sim 40$).

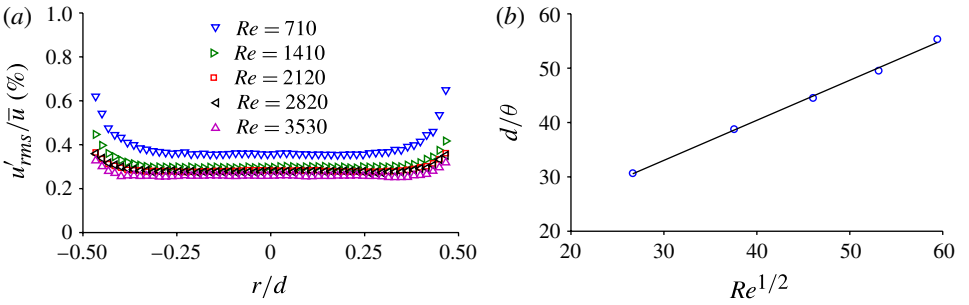

FIGURE 1. (Colour online) Baseflow characteristics: (*a*) turbulence intensity as a function of radial position and (*b*) transverse curvature as a function of the square root of the Reynolds number. The data are from a hot wire positioned at the injector outlet ($x/d \approx 0$). The linear fit in (*b*) shows that the shear layers are initially laminar.

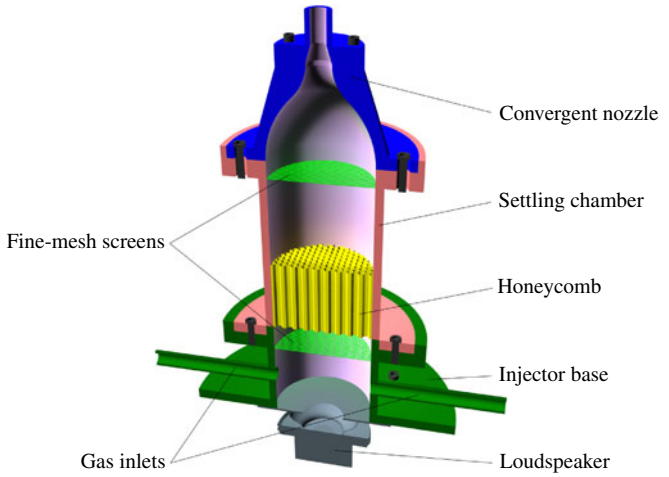

FIGURE 2. (Colour online) Cross-section of the injector used to create a hydrodynamically self-excited jet.

Guided by these parameters, we create our self-excited jet by discharging helium gas from a convergent nozzle. In ambient air, helium has a density ($S = 0.14$) well below the upper threshold for global instability, which ranges between $S \approx 0.61$ and 0.73 in most experiments, such as those by Monkewitz *et al.* (1990) and Kyle & Sreenivasan (1993). The convergent nozzle ensures that this instability can be easily distinguished from background noise. It does this in two ways: (i) by creating a velocity profile with thin shear layers, which reduces the critical Reynolds number and, hence, the amplification of inherent disturbances by convective modes (Hallberg *et al.* 2007); and (ii) by ensuring that the baseflow itself is quiet and that its shear layers are laminar (Mehta & Bradshaw 1979). As figure 1 shows, for $Re \leqslant 3.5 \times 10^3$, the turbulence intensity in the jet core is low ($u'_{rms}/\overline{u} < 0.37\,\%$) and the transverse curvature scales as $d/\theta \propto Re^{1/2}$ (with θ integrated to $\overline{u}/\overline{u}_{max} = 0.1$), indicating that the shear layers are indeed initially laminar. This nozzle is part of an injector assembly (figure 2) that was loaned to us by Daniel Durox from École centrale de Paris. It has a round $d = 6$ mm

diameter outlet and a contraction area ratio of 52:1. For flow conditioning, it has a set of fine-mesh screens and honeycomb in its settling chamber, as described by Li (2011).

We force the jet sinusoidally in time with a loudspeaker mounted upstream. We do this over a range of frequencies ($0.84 \lesssim f_f/f_n \lesssim 1.16$) around the natural global frequency, f_n, in order to study 1:1 (primary) lock-in. These frequencies ($823 \leqslant f_f \leqslant 1143$ Hz) are sufficiently far from the Helmholtz resonance frequency of the injector (380 Hz with helium) that the gain of the forcing system is relatively constant. The acoustic wavelengths are sufficiently longer than the characteristic jet length scale ($c_\infty/f_f d \gg 1$) that the perturbations are spatially coherent. At each forcing frequency, f_f, we incrementally increase the forcing amplitude, A, until just beyond the onset of lock-in. We define A as the peak-to-peak voltage into the loudspeaker (in units of $\mathrm{mV_{pp}}$), so that it is directly proportional to the acoustic pressure amplitude and to the square root of the acoustic power.

We measure the jet response with a hot-wire anemometer. We verify that the data are unaffected by the physical presence of the probe with flow visualization (described later) and simultaneous near-field pressure measurements. The probe consists of a 5 μm diameter tungsten wire, which we calibrate in both helium and air, using the procedure of Johnson, Uddin & Pollard (2005), to a nominal uncertainty of ±1.7 % at 95 % confidence on the normal distribution. We operate the probe in constant-temperature mode, at an overheat ratio of 1.8, for a maximum spectral response of 10^4 Hz, which is at least one order of magnitude higher than the expected flow frequencies. According to Broze & Hussain (1994), a global mode tends to coordinate the motion of an entire streamwise region such that its dynamics become primarily temporal and can be characterized by measurements at a fixed location. For most of our measurements, therefore, we position the probe on the jet centreline, $1.5d$ downstream of the injector outlet (i.e. at $(x/d, r/d) = (1.5, 0)$) with an uncertainty of $\pm 0.017d$ in each axis. We choose this sampling location for two reasons: (i) it is sufficiently far downstream that the global mode, whose amplitude peaks at $x/d \approx 2$ for our test conditions, has time to grow and interact with the upstream forcing; but (ii) it is not so far downstream that it is outside the potential core, which means that we can use the bridge calibration for helium without the need to account for local fluctuations in mass fraction. At each forcing condition, we digitize the hot-wire voltage at 16 384 Hz for 16 s on a 16-bit data converter, producing a time series of the streamwise velocity. This sampling duration is sufficiently long for data stationarity: (i) it is four orders of magnitude longer than the time scale of the natural jet oscillations; (ii) it is three orders of magnitude longer than the longest time scale of the forced jet oscillations (which is due to beating, see § 3.2.1); but (iii) it is not so long that slow variations in the ambient conditions can cause significant parametric drifts in the system, e.g. in its natural frequency. From the time series, we compute the PSD using the algorithm of Welch (1967), with Hamming windows to reduce spectral leakage, resulting in a frequency resolution of 0.25 Hz.

For flow visualization, we use schlieren imaging (Settles 2001). Our optical set-up consists of two concave parabolic mirrors (152.4 mm in diameter and 1219 mm in focal length) aligned in a Z-type Herschelian configuration. It receives illumination from a light-emitting diode, collimates this through the jet and then focuses the output onto a knife edge and into a high-speed digital camera (Phantom V4.2).

2.2. *Modelling*

As noted in § 1, several researchers, including Huerre & Monkewitz (1990), have suggested that open self-excited flows are amenable to low-dimensional modelling, using analogies similar to those which have previously been demonstrated for closed flows in small-aspect-ratio geometries (e.g. Taylor–Couette flow; Mullin & Price 1989). We therefore model our forced jet system with the forced VDP oscillator, a three-dimensional nonlinear dynamical system first studied by van der Pol & van der Mark (1927). We use this particular oscillator because it is one of the simplest but most well-analysed models with self-excited temporal solutions (see the book by Balanov *et al.* 2009). As in the experiments, the forcing is external and sinusoidal:

$$\ddot{z} - \epsilon(1 - z^2)\dot{z} + \omega_0^2 z = B\sin(\omega_f t), \tag{2.1}$$

where z is the dynamical variable and ω_0 is the angular frequency at which it would oscillate in the absence of feedback ($\epsilon = 0$) and forcing ($B = 0$). The forcing has an amplitude of B and an angular frequency of ω_f. The feedback parameter, ϵ, controls the degree of both linear self-excitation (power supply) and nonlinear self-limitation (power dissipation). For $\epsilon = 0$ (and $B = 0$), there is neither and the system becomes a simple harmonic oscillator. For $\epsilon > 0$ (and $B = 0$), there is a fixed point at $z = \dot{z} = 0$ but, because it is unstable (via a Hopf bifurcation at $\epsilon = 0$), the system tends to a limit cycle. This occurs through successive changes in the sign of the damping coefficient, $-\epsilon(1 - z^2)$, as z oscillates. When the amplitude is small ($|z| < 1$), this coefficient is negative, causing self-excitation and growth. When the amplitude is large ($|z| > 1$), it is positive, causing self-limitation and decay. The system thus alternates between positive and negative damping as z oscillates. Eventually, the positive damping cancels out the negative damping over a cycle, causing the system to settle into a limit cycle.

For $\epsilon \ll 1$ (and $B = 0$), the system has weak nonlinearity and its phase trajectory (to be defined in § 2.3) is almost a perfect circle. For $\epsilon \gg 1$ (and $B = 0$), the system has strong nonlinearity and its phase trajectory is no longer circular. Instead, it exhibits relaxation oscillations, described by van der Pol (1926) as periodic oscillations that have a slow gradual buildup followed by a fast sudden discharge (or vice versa). Regardless of the degree of nonlinearity, however, the (unforced) system always settles into a stable limit cycle, which attracts all other trajectories regardless of their initial conditions, i.e. the entire phase plane is a basin of attraction for this periodic attractor.

In § 3.2, we will study how this limit cycle of the VDP oscillator is affected by external forcing ($B > 0$). We will use this as an analogy for how the limit cycle of the low-density jet is affected by similar forcing ($A > 0$). We fix the feedback parameter at a small value of $\epsilon = 0.2$ for reasons that will become clear in § 3.2.3. We leave ω_0 at 1 but note that this value is not necessarily equal to the natural angular frequency of the actual nonlinear ($\epsilon > 0$) oscillations, which we will call ω_n. We solve the system (2.1) numerically using a multistep variable-order algorithm (Shampine & Reichelt 1997). We do this for a range of forcing frequencies and amplitudes in order to replicate the experimental conditions.

2.3. *Nonlinear time-series analysis*

As noted above, both the jet and the VDP oscillator are self-excited systems. This means that their dynamics are governed by nonlinear processes and cannot be adequately described with linear tools operating in the time or frequency domain. Instead, nonlinear tools operating in the state domain must be used, one of the most powerful of which is nonlinear time-series analysis (NTSA). Developed from the

theory of dynamical systems, NTSA has been continually refined since the 1980s and is now a relatively mature and reliable tool, as demonstrated by the many books on the subject, such as those by Kantz & Schreiber (2003) and Small (2005). In this paper, we apply NTSA to both the jet and the VDP oscillator in order to describe and compare their nonlinear dynamics.

The first step of NTSA is to determine the phase space. For a continuous dynamical system, this is a D-dimensional hyperspace containing all D state variables. Within it, the state of the system, at any given time, is represented by a discrete point. As the system evolves, the active points trace out a continuous path, known as the phase trajectory. According to Strogatz (1994), the features of this trajectory can provide useful insight into the topology of the attractor (the set approached as $t \to \infty$) and, hence, into the underlying dynamics. If the system is periodic, for example, its trajectory is an isolated closed orbit around a periodic attractor. If it is quasiperiodic, its trajectory is a non-repeating orbit around a torus attractor. If it is chaotic, its trajectory is a non-repeating orbit around one or more strange attractors (self-similar fractals).

For most physical systems, the phase space cannot be directly measured because the state variables within it are neither known nor measurable. Fortunately, though, many such variables are intrinsically coupled to each other. This means that, through the use of time-delay embedding (Takens 1981), the phase space can be reconstructed from a generic observation function, typically just a single scalar time series, which is either measured in experiments or computed in simulations. In our analysis, we follow this procedure by unfolding the original attractor into an m-dimensional Euclidean vector of time-delayed elements formed from our data:

$$\boldsymbol{\xi}(t) = [u'(t), u'(t-\tau), u'(t-2\tau), \ldots, u'(t-(m-1)\tau)], \quad \boldsymbol{\xi} \in \mathbb{R}^m, \tag{2.2}$$

where u' is the jet velocity fluctuation (for the VDP oscillator, this is replaced by z'). For an accurate reconstruction, both the time delay, τ, and the embedding dimension, m, must be carefully chosen. If τ is too small, the vector elements become strongly correlated, accumulating along the bisectrix of the embedding space. If τ is too large, they become weakly correlated owing to numerical inaccuracies and noise, appearing randomly distributed. The optimal time delay is that which maximizes the unfolding of the attractor in all embedding dimensions and thus provides the most information about the dynamics. To find this value, we follow the suggestion of Fraser & Swinney (1986) by calculating the average mutual information. This is a quantity taken from the field of information theory and its use in NTSA is standard. According to Kantz & Schreiber (2003), its key advantage over other similar quantities is that it accounts for nonlinear correlations, not just linear ones. Mathematically, it is a statistical measure of the average amount of information that can be predicted about $u'(t-\tau)$ from the original signal $u'(t)$:

$$I(\tau) = \sum_{i=1}^{n} P[u'(t_i) \cap u'(t_i-\tau)] \log_2 \frac{P[u'(t_i) \cap u'(t_i-\tau)]}{P[u'(t_i)]P[u'(t_i-\tau)]}, \tag{2.3}$$

where n is the number of samples and P is the standard notation for probability. For example, $P[u'(t_i)]$ is the probability that $u'(t)$ has a value $u'(t_i)$, and $P[u'(t_i) \cap u'(t_i-\tau)]$ is the analogous joint probability. Fraser & Swinney (1986) recommend that the time delay for reconstruction be set to the time required by $I(\tau)$ to reach its first minimum, because this is when the delayed elements are least predictable and, hence, most informative. Applying this criterion (figure 3*a*), we find that, for both of our self-

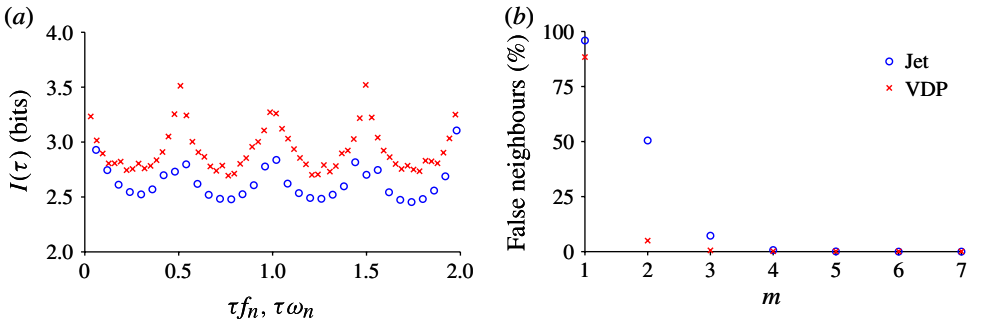

FIGURE 3. (Colour online) Optimal parameters for phase-space reconstruction: (*a*) average mutual information as a function of the time delay and (*b*) false nearest neighbours as a function of the embedding dimension, both for the jet and the VDP oscillator. In (*a*) the time delay is normalized by the natural oscillation period.

excited systems, the optimal time delay is about one-third of the natural oscillation period. We find the same result for the forced cases (not shown). Incidentally, this value of τ concurs with that found by using the first zero-crossing of the autocorrelation function, which is another common, albeit linear, way of choosing the optimal time delay (Abarbanel 1996).

The embedding dimension, m, is the dimension of the hyperspace onto which the original phase space is projected. Its value must be sufficiently large in order for the reconstructed attractor to be a one-to-one projection of the original attractor. Achieving this is crucial to ensuring that the dynamical invariants of the system, such as generalized dimensions and other topological properties, are preserved. Otherwise, if m is too small, points are falsely projected into the neighbourhood of other points, creating false neighbours, thus causing the phase trajectory to cross itself. According to Takens (1981), the minimum value of m required for a one-to-one projection depends on the number of DOFs in the system. For most physical systems, only a few DOFs remain active in the limit $t \to \infty$. This means that the dominant attractor occupies only a small subspace and that m need not be as large as the full phase-space dimension. However, m must be larger than twice the attractor dimension (Takens 1981), i.e. larger than twice the topological dimension of the manifold on which the effective dynamics occurs. This dimension can be estimated with the correlation dimension (appendix A), although most algorithms for this still use m as a user-defined input.

To find the minimum value of m required, we use the method of false nearest neighbours, as proposed by Kennel, Brown & Abarbanel (1992). This involves calculating the percentage of false neighbours as a function of m and then finding the value of m above which this percentage is near zero. Applying this method (figure 3*b*), we find just a few false neighbours for $m = 3$ and almost none for $m \geqslant 4$. This means that a three-dimensional projection is sufficient to resolve the main features of the attractor, but that at least a four-dimensional projection is required to resolve all of the detailed features. In our reconstruction, therefore, we use $m = 7$ to calculate quantitative information, such as the correlation dimension (appendix A). However, we use $m = 3$ to visualize qualitative information, such as the attractor structure (§§ 3.2.1 and 3.2.2). In particular, we make a transverse cut through the (three-dimensional) phase trajectory formed by (2.2) and then inspect the intercepts

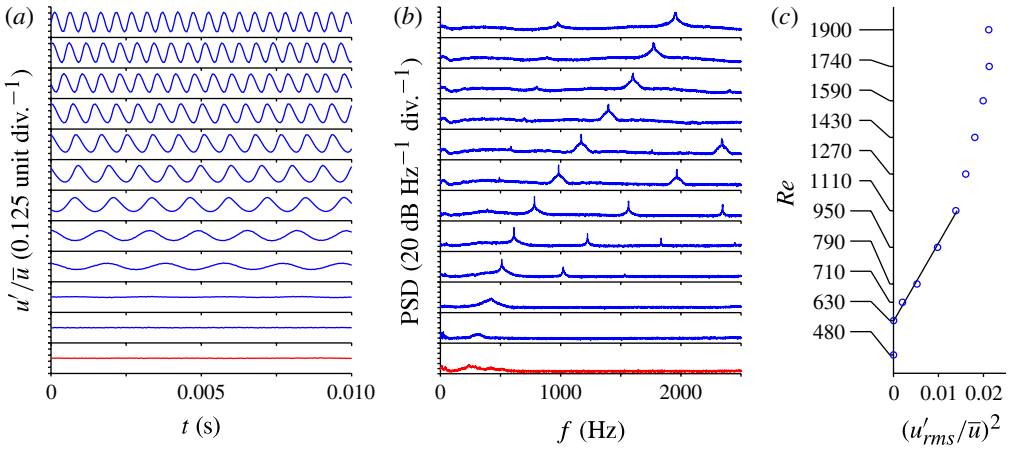

FIGURE 4. (Colour online) Natural jet dynamics: (*a*) time trace, (*b*) PSD and (*c*) squared amplitude of velocity fluctuations in the low-density jet at $480 \leqslant Re \leqslant 1900$ and in an equidensity jet at $Re = 1410$ (shown at the bottom, in red online). The data are from a hot wire positioned at $(x/d, r/d) = (1.5, 0)$. In (*c*), which has linear axes and contains data from only the low-density jet, the linear increase in $(u'_{rms}/\overline{u})^2$ for $630 \leqslant Re \leqslant 1110$ indicates a supercritical Hopf bifurcation to a global mode.

for information about the topology and geometry. For clarity, we consider a section of the cut that contains only (one-way) intercepts of the trajectory with the plane $u'(t-2\tau) = 0^+$. This section is called a (one-sided) Poincaré map, on which every class of nonlinear response has its own characteristic features. For example, a periodic limit cycle, whose trajectory is a closed orbit, appears as a point. A quasiperiodic oscillation with two incommensurate modes, whose trajectory is a non-repeating orbit on a two-dimensional torus $\mathbb{T}^2$, appears as a continuous ring. (A quasiperiodic trajectory never repeats itself because its orbital period about the major toroidal axis is not a rational multiple of its orbital period about the minor toroidal axis. Its intercept with the Poincaré plane therefore drifts from cycle to cycle, never returning to the same point. Over many cycles, it gradually fills in a closed curve, forming a continuous ring, which is sometimes called a drift ring.)

3. Results

3.1. *Natural global bifurcation of the jet*

Before examining the forced jet response, we must first find an unforced operating condition that supports global instability. Because S is fixed by the use of helium, there are in theory two control parameters (§ 2.1): Re and d/θ. Because our injector geometry is also fixed, however, these two parameters are coupled to each other ($d/\theta \propto Re^{1/2}$, figure 1*b*), leaving just one independent control parameter: Re.

In figure 4, we show the time trace, PSD and squared amplitude of velocity fluctuations from the low-density jet for 11 Reynolds numbers: $480 \leqslant Re \leqslant 1900$. For comparison, we also show the same quantities (except the squared amplitude) from an equidensity jet ($S = 1$) for an intermediate Reynolds number: $Re = 1410$. We define the squared amplitude as the square of the root-mean-square (r.m.s.) velocity fluctuation normalized by the time-averaged velocity: $(u'_{rms}/\overline{u})^2$.

For the equidensity jet, the PSD contains broadband noise, with a slight increase around 250 Hz but no clear peak. This is because the jet is marginally globally stable (Ho & Huerre 1984): the global mode is lightly damped, with a temporal growth rate just below zero. The broadband spectrum indicates that neither acoustical nor mechanical resonance of the injector is strong enough to cause oscillations.

For the low-density jet, the PSD at $Re = 480$ resembles that for the equidensity jet: there is a slight increase around a few hundred Hertz but no clear peak. This is because the jet is not globally unstable at this Reynolds number, i.e. the inertia of small perturbations is not sufficient to overcome the stabilizing effect of viscosity. The behaviour at $Re = 630$ is marginal but, at $Re = 710$, a sharp peak emerges in the PSD, along with its harmonics. This indicates that the jet has become globally unstable, behaving as a self-excited oscillator with an intrinsic natural frequency, rather than as a spatial amplifier of extrinsic perturbations. This hydrodynamic oscillator sustains its limit-cycle motion against dissipation by continually extracting power from the baseflow through the action of baroclinicity (Lesshafft & Huerre 2007). Its natural frequency increases with Re according to the scaling proposed by Hallberg & Strykowski (2006) using a viscous diffusion time scale.

Close to criticality ($630 \leqslant Re \leqslant 1110$), the squared amplitude, $(u'_{rms}/\overline{u})^2$, increases linearly with Re. This is the classical behaviour near a supercritical Hopf bifurcation, which can be modelled with a Landau equation containing just first- and third-order terms (Provansal *et al.* 1987; Monkewitz *et al.* 1990). Far from criticality ($1270 \leqslant Re \leqslant 1900$), the increase is less than linear, as higher-order effects become influential.

These results show that a wide range of operating conditions in our experimental facility can lead to global instability in a low-density axisymmetric jet. For the forcing tests that follow (§ 3.2), we will focus on just one operating condition: $Re = 1110$, $d/\theta = 35.5$ and $S = 0.14$. We choose this particular condition for four reasons: (i) it is sufficiently far from the bifurcation point that, even with strong forcing, the instantaneous Re remains above criticality; (ii) it is not so far from the bifurcation point that lock-in becomes unachievable with our forcing system; (iii) its Richardson and Mach numbers are sufficiently low ($Ri \equiv gd(\rho_\infty - \rho_j)/\rho_j U_j^2 = 7.4 \times 10^{-4}$ and $M \equiv U_j/c_\infty = 6.5 \times 10^{-2}$) that buoyancy and compressibility effects are negligible (Subbarao & Cantwell 1992); and (iv) its transverse curvature is in a range that gives rise to absolute instability for the axisymmetric mode but not for any of the helical modes (Jendoubi & Strykowski 1994; Hallberg *et al.* 2007; Lesshafft & Huerre 2007). The helical modes are more geometrically complex and could compete with the axisymmetric mode for control of the global oscillations, potentially distorting their motion and complicating the interpretation of the PSD and Poincaré map.

At this operating condition, the global mode consists of axisymmetric (varicose) structures in the near field, oscillating within an intact potential core (figure 5). With downstream development, however, these structures break down, starting with an abrupt termination of the potential core ($x/d \approx 2.5$), followed by the three-dimensional formation of side jets (which arise from secondary instabilities; Nichols, Chomaz & Schmid 2007), and ending in turbulence in the far field. Because we position our hot wire upstream of this breakdown (§ 2.1), we obtain relatively clean measurements of the dynamics of the intrinsic wavemaker, which local stability analyses show sits at the injector plane (Monkewitz, Huerre & Chomaz 1993; Chomaz 2005; Lesshafft *et al.* 2006), including its response to upstream forcing.

When unforced, the global mode has a natural frequency of $f_n = 983.0$ Hz $\pm$ 0.15 % and a Strouhal number of $St_n \equiv f_n d/U_j = 0.27 \pm 3.0\,\%$, both at 95 % confidence on

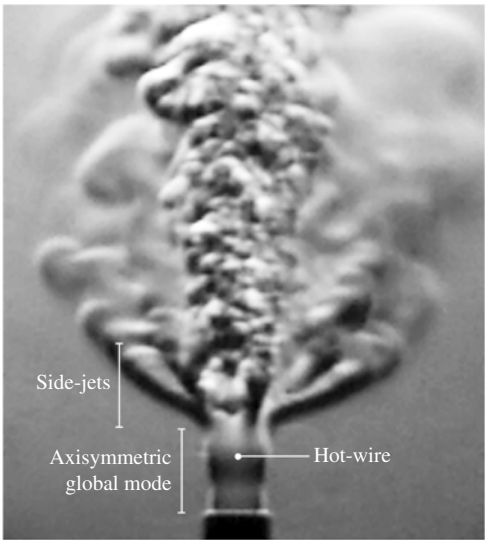

FIGURE 5. Schlieren snapshot of the unforced low-density jet at the operating condition of our forcing tests: $Re = 1110$, $d/\theta = 35.5$ and $S = 0.14$ (helium in air). The axisymmetric global mode is visible around the potential core, upstream of the side jets. The hot wire is positioned at $(x/d, r/d) = (1.5, 0)$ with its holder parallel to the jet axis.

the t-distribution of Student (1908). When forced, however, the global mode has a natural frequency, f_n^*, whose value can shift from its unforced value (f_n, without an asterisk), as we will see in § 3.2. According to Hilborn (2000), this shifting, or pulling, as it is often called (Koepke & Hartley 1991), of the natural frequency is a characteristic feature of forced nonlinear oscillators. In the literature, it is quantified using both the bare winding number, f_n/f_f, and the dressed winding number, f_n^*/f_f. In the sections to follow, we will use similar ratios, but in inverse or rescaled form, for similar and related purposes. However, we will always express them as rational numbers, not because they necessarily are, but because we must round them to the significant digits required by the finite precision of the PSD measurements. (Numerical simulations suffer from a similar artefact in that floating point numbers are necessarily rational.) On examining the forced response (§ 3.2), we will find that, at the resolution of our phase-space reconstruction, all such ratios arising from our test conditions (except lock-in) can be considered irrational, i.e. incommensurate. This distinction is important for determining quasiperiodicity and for distinguishing it from very long periodicity.

3.2. *Forced response of the jet and the VDP oscillator*

Having chosen a suitable operating condition, we proceed to examine the forced response of the jet and to compare this to that of the VDP oscillator.

3.2.1. *Leading up to lock-in: f_f close to f_n* ($|1 - f_f/f_n| \lesssim 0.07$)

First we consider the jet when it is forced at a frequency slightly above its natural frequency: $f_f/f_n = 1023\ \text{Hz}/983\ \text{Hz} \approx 1.04$. In figure 6(*a–c*), we show the time trace, PSD and Poincaré map of its velocity fluctuation for eight forcing amplitudes: $300 \leqslant A \leqslant 900\ \text{mV}_{\text{pp}}$. For comparison, we also show the same quantities without forcing. We find that the jet exhibits a range of nonlinear dynamics:

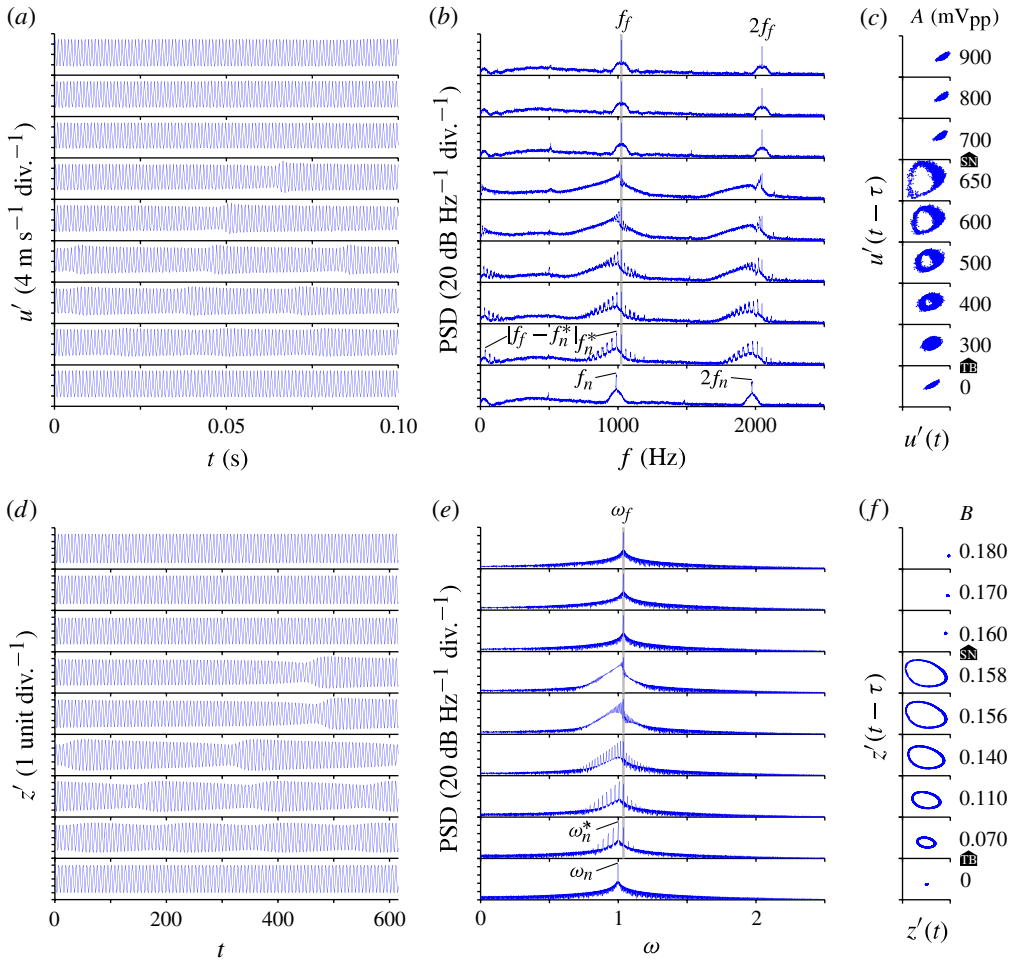

FIGURE 6. (Colour online) Forced response of (*a–c*) the jet and (*d–f*) the VDP oscillator for a forcing frequency slightly above the natural frequency: $f_f/f_n = \omega_f/\omega_n \approx 1.04$. For both systems, the (*a,d*) time trace, (*b,e*) PSD and (*c,f*) Poincaré map are shown for eight forcing amplitudes and for the unforced case. The transition from periodicity to quasiperiodicity occurs via a torus-birth bifurcation: see the arrows labelled TB ($A = 0 \rightarrow 300\ \mathrm{mV_{pp}}$; $B = 0 \rightarrow 0.070$). The transition from quasiperiodicity to lock-in occurs via a saddle-node bifurcation with frequency pulling: see the arrows labelled SN ($A = 650 \rightarrow A_{loc} = 700\ \mathrm{mV_{pp}}$; $B = 0.158 \rightarrow B_{loc} = 0.160$).

(i) When unforced ($A = 0\ \mathrm{mV_{pp}}$), it has a global mode at a discrete natural frequency, represented in the PSD by a sharp peak at $f_n = 983$ Hz. This is accompanied by similar, but weaker, peaks at its harmonics (both even and odd), indicating that the natural varicose oscillations are not perfectly sinusoidal in time. In particular, the peak at the first subharmonic, $f_n/2 = 491.5$ Hz, suggests a period-doubling motion, commonly associated with vortex pairing. In the Poincaré map, the data points are clustered around one blob. This indicates that the phase trajectory is closed, confirming that the jet oscillates periodically in a limit cycle. If the oscillations were free of cyclic variability, the trajectory would be perfectly closed and the

Poincaré map would show one discrete point. The source of this variability is background noise, as our calculations of the correlation dimension show no evidence of a low-dimensional strange attractor (appendix A).

(ii) When forced at low amplitudes ($300 \leqslant A \leqslant 400$ mV$_{pp}$), the jet responds at f_f as well as f_n^*, the natural frequency modified by the forcing. It also responds at several different frequencies around these two incommensurate frequencies, as indicated by the spectral peaks at their linear combinations (i.e. $|pf_f \pm qf_n^*|$, with p and q as integers). Known as sidebands, these peaks are caused by nonlinear wave–triad interactions between the forced and natural modes (Craik 1988). Their presence suggests that the jet has become quasiperiodic via a torus-birth (Neimark–Sacker) bifurcation, behaving like a typical forced oscillator before lock-in (Nayfeh & Balachandran 2004). This is confirmed by the Poincaré map: the emergence of a continuous ring indicates that the phase trajectory is no longer closed, but spirals around the surface of a stable ergodic $\mathbb{T}^2$ torus attractor (Kuznetsov 2004). The bifurcation is also confirmed by the correlation dimension (appendix A): over a range of intermediate Euclidean scales, this attractor invariant does indeed approach two, the value for quasiperiodicity with two incommensurate modes. Finally, there are additional spectral peaks at low frequencies, $f < 100$ Hz. Among them, the strongest corresponds to the beat frequency, $|f_f - f_n^*|$. In the time trace, this beating phenomenon can be seen as low-frequency (long-wavelength) modulations of the velocity amplitude.

(iii) When forced at moderate amplitudes ($500 \leqslant A \leqslant 650$ mV$_{pp}$), the jet continues to respond at both f_f and f_n^*, as well as at several nearby frequencies. However, f_n^* is increasingly pulled towards f_f, which remains fixed. This decrease in $|f_f - f_n^*|$ causes an equal decrease in the main beat frequency. Meanwhile, the spectral peaks around f_f and f_n^* become closer and their envelope widens. By $A = 650$ mV$_{pp}$, they are almost imperceptible (within the limits of the PSD resolution) and their envelope is biased towards low frequencies, as indicated by the longer tail. In the Poincaré map, the ring grows as A increases, confirming that the jet is still quasiperiodic.

(iv) When forced above a critical amplitude ($A \geqslant A_{loc} = 700$ mV$_{pp}$), the jet locks into the forcing. The PSD becomes dominated by f_f and its harmonics, with no sign of the original natural mode. The time trace shows that the velocity amplitude is no longer modulated. In the Poincaré map, the ring collapses to another blob, indicating that the phase trajectory collapses to another periodic orbit. The abruptness of this collapse suggests that the torus attractor is not dead, but has become resonant via a saddle-node (blue-sky) bifurcation, which means that it now contains periodic orbits on its surface. As we will see shortly, this interpretation of the dynamics is consistent with an analysis of the VDP oscillator performed by Balanov *et al.* (2009). According to this analysis, the onset of (1:1) lock-in occurs when the phase trajectory locks into a stable periodic orbit on the resonant torus surface. Once locked-in, the jet behaves like the unforced jet, except that its limit-cycle frequency is f_f instead of f_n.

When the VDP oscillator is forced at the same frequency ($\omega_f/\omega_n = 1.038/0.998 \approx 1.04$), it responds qualitatively like the jet. This is clear from figure 6(*d–f*), in which we show the time trace, PSD and Poincaré map of the steady-state solution for eight forcing amplitudes: $0.070 \leqslant B \leqslant 0.180$. For comparison, we also show the same quantities without forcing. We find striking similarities between the jet and the VDP oscillator:

(i) When unforced ($B = 0$), the VDP oscillator has a dominant natural frequency, represented in the PSD by a sharp peak at $\omega_n = 0.998$, which is slightly less than $\omega_0 = 1$ owing to nonlinearity (Guicking & Haars 1991). There are, however, no even harmonics, only odd ones (not shown). These are weak because the cubic nonlinear term is small ($\epsilon = 0.2$) and, hence, the solution is nearly sinusoidal in time. The Poincaré map shows one discrete point, indicating that the phase trajectory is closed, confirming that the solution is a periodic limit cycle.

(ii) When forced at low amplitudes ($0.070 \leqslant B \leqslant 0.110$), the VDP oscillator responds at ω_f as well as ω_n^*, with multiple components around these but none at the beat frequency. The Poincaré map shows a continuous ring, indicating that the phase trajectory spirals around the surface of a stable ergodic $\mathbb{T}^2$ torus attractor (Kuznetsov 2004). Thus, like the jet, the VDP oscillator becomes quasiperiodic via a torus-birth bifurcation.

(iii) When forced at moderate amplitudes ($0.140 \leqslant B \leqslant 0.158$), the VDP oscillator continues to respond at both ω_f and ω_n^*, as well as at several nearby frequencies. It exhibits the same pulling of ω_n^* towards ω_f as in the jet, with the same bias of the PSD envelope towards low frequencies. In the Poincaré map, the ring grows as B increases, confirming that the solution is still quasiperiodic.

(iv) When forced above a critical amplitude ($B \geqslant B_{loc} = 0.160$), the VDP oscillator locks into the forcing. This occurs because its topology changes. To show this, Balanov *et al.* (2009) transformed the original forced VDP equation (2.1) into an autonomous system, thereby reducing the analysis of periodic orbits to an analysis of fixed points. At these fixed points, both the amplitude of the forced oscillations and the phase difference between them and the forcing do not vary with time. To explore lock-in, the researchers searched for a stable fixed point, i.e. a stable periodic orbit. They found one emerging as the torus attractor became resonant via a saddle-node bifurcation. This analytical finding concurs not only with our numerical VDP data (figure 6*d–f*: $B = 0.158 \rightarrow 0.160$) but also with our experimental jet data (figure 6*a–c*: $A = 650 \rightarrow 700$ $\mathrm{mV_{pp}}$). For both systems, the ring in the Poincaré map collapses abruptly at lock-in, indicating a sudden loss of stability in the torus attractor but not its death. In particular, the analysis of Balanov *et al.* (2009, figure 3.11) predicts that a pair of fixed points, one stable and one saddle, emerges on the resonant torus surface, with the stable one being a periodic orbit at ω_f. Inside the torus lies an existing (third) fixed point, which arises from the natural mode but is unstable; it was initially stable before forcing was applied ($B = 0$) but became unstable after the torus-birth bifurcation to quasiperiodicity. After lock-in, as B increases above B_{loc}, this unstable fixed point collides with the saddle fixed point on the torus surface, causing both of them and the torus itself to disappear via another saddle-node bifurcation. Meanwhile, the stable fixed point, to which the phase trajectory has converged, is unaffected, which means that this last bifurcation would be undetectable in simulations or experiments. This is another analytical finding that concurs with our numerical VDP data (figure 6*d–f*: $B = 0.160 \rightarrow 0.180$) and experimental jet data (figure 6*a–c*: $A = 700 \rightarrow 900$ $\mathrm{mV_{pp}}$).

In both the jet and the VDP oscillator, the above sequence of dynamics arises not just when the forcing frequency is above the natural frequency, but also when it is below it. For example, figure 7 is analogous to figure 6 but for $f_f/f_n = \omega_f/\omega_n \approx 0.96$ (instead of 1.04). It shows that, regardless of the relative value of the two frequencies (as long as they are close together, which we will explain in § 3.2.2), the forced

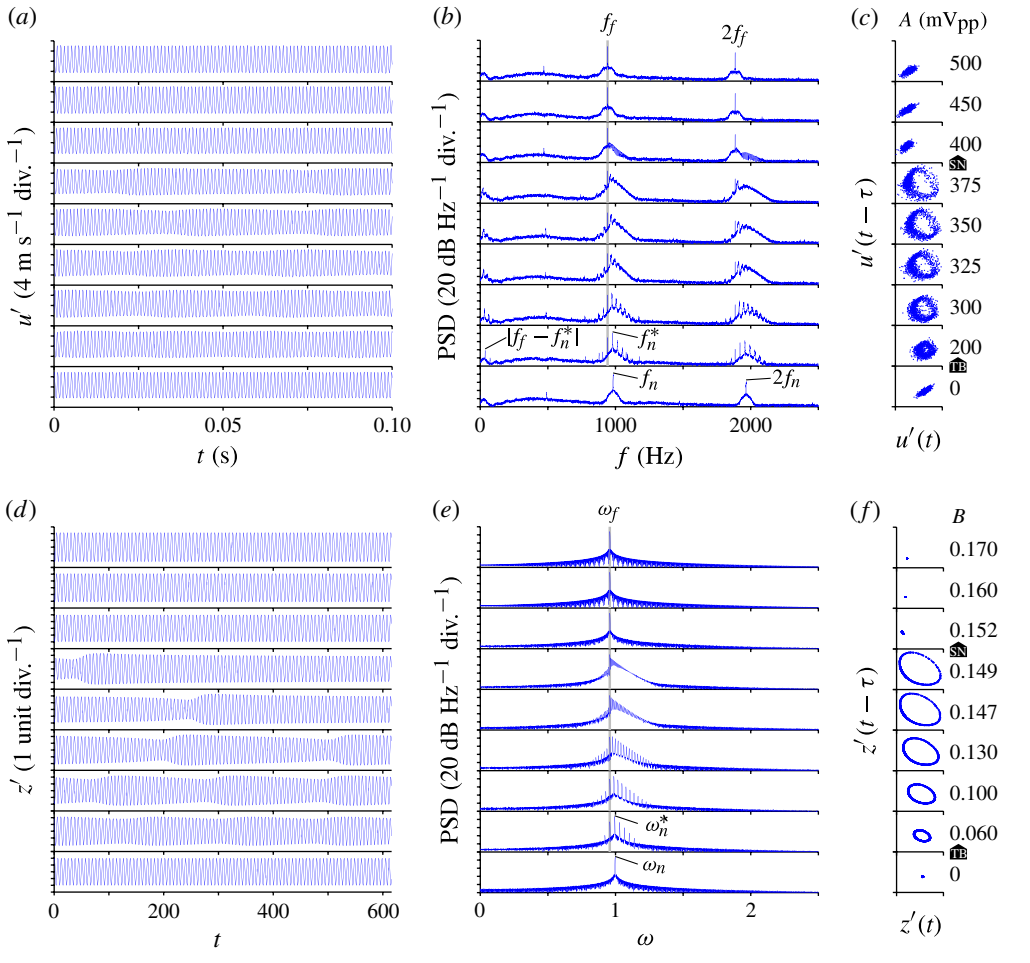

FIGURE 7. (Colour online) Forced response of (*a–c*) the jet and (*d–f*) the VDP oscillator for a forcing frequency slightly below the natural frequency: $f_f/f_n = \omega_f/\omega_n \approx 0.96$. For both systems, the (*a,d*) time trace, (*b,e*) PSD and (*c,f*) Poincaré map are shown for eight forcing amplitudes and for the unforced case. The transition from periodicity to quasiperiodicity occurs via a torus-birth bifurcation: see the arrows labelled TB ($A = 0 \to 200\ \mathrm{mV_{pp}}$; $B = 0 \to 0.060$). The transition from quasiperiodicity to lock-in occurs via a saddle-node bifurcation with frequency pulling: see the arrows labelled SN ($A = 375 \to A_{loc} = 400\ \mathrm{mV_{pp}}$; $B = 0.149 \to B_{loc} = 0.152$).

response leading up to lock-in is qualitatively similar. This implies (i) for no forcing, a periodic limit cycle at the natural frequency; (ii) for weak forcing, a torus-birth bifurcation to quasiperiodicity; (iii) for moderate forcing, a bias of the PSD envelope and a growth of the torus attractor; and (iv) for strong forcing, a saddle-node bifurcation to lock-in.

Crucially, these similarities also include frequency pulling (or phase pulling; Dewan 1972): the pulling of the natural frequency towards the forcing frequency as the forcing amplitude increases towards the critical value for lock-in. To explore this, we show in figure 8 the frequency-pulling ratio, $\phi \equiv |f_f - f_n^*|/|f_f - f_n|$ for the jet or $\phi \equiv |\omega_f - \omega_n^*|/|\omega_f - \omega_n|$ for the VDP oscillator, as a function of the normalized forcing

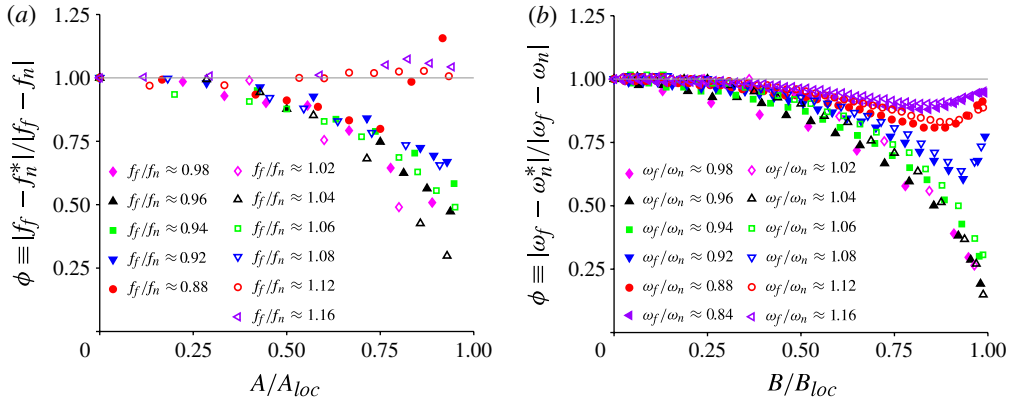

FIGURE 8. (Colour online) Frequency-pulling ratio as a function of the forcing amplitude for (*a*) the jet and (*b*) the VDP oscillator. Data are shown for a range of forcing frequencies, with hollow markers denoting $f_f/f_n = \omega_f/\omega_n > 1$ and filled markers denoting $f_f/f_n = \omega_f/\omega_n < 1$.

amplitude, A/A_{loc} or B/B_{loc}. This ratio (ϕ) is like a rescaled version of the dressed winding number (f_n^*/f_f or ω_n^*/ω_f; Hilborn 2000) in that it accounts for changes in the actual frequency of oscillation due to nonlinear coupling. Once again, we find striking similarities, but also subtle differences, between the jet and the VDP oscillator:

(i) When forced close to the natural frequency ($|1 - f_f/f_n| = |1 - \omega_f/\omega_n| \lesssim 0.07$), both systems exhibit frequency pulling up to lock-in: ϕ starts at 1 and decreases towards 0 as A/A_{loc} or B/B_{loc} increases. For the jet (figure 8*a*), there appears to be significant scatter at the higher forcing amplitudes ($0.75 \leqslant A/A_{loc} \leqslant 1$), but most of this can be attributed to two systematic factors. The first is an asymmetry about $f_f/f_n = 1$: for a given difference between f_f and f_n, frequency pulling is stronger for $f_f/f_n > 1$ (hollow markers) than it is for $f_f/f_n < 1$ (filled markers). This asymmetry is strongest when f_f/f_n is near 1, and weakens as f_f/f_n deviates from 1. The second factor is a bias towards $f_f/f_n = 1$: for either $f_f/f_n > 1$ or $f_f/f_n < 1$, frequency pulling is strongest when f_f/f_n is near 1, and weakens as f_f/f_n deviates from 1. For the VDP oscillator (figure 8*b*), there is less scatter because both of these factors are less dominant.

(ii) When forced far from the natural frequency ($|1 - f_f/f_n| = |1 - \omega_f/\omega_n| \gtrsim 0.07$), both systems exhibit frequency pulling but not up to lock-in: ϕ decreases from 1, reaches a minimum and then increases back towards 1 as A/A_{loc} or B/B_{loc} increases. Moreover, as the forcing frequency deviates from the natural frequency, the minimum in ϕ shifts to lower forcing amplitudes and its value increases, indicating weaker frequency pulling. Although these trends are clear in the VDP data, they are much less clear in the jet data, particularly at $f_f/f_n \approx 0.92$ and 1.08. For these two cases, we speculate that the discrepancy arises from a lack of resolution in A/A_{loc} near $A/A_{loc} = 1$: ϕ for the jet probably returns to 1 just before lock-in, as it does for the VDP oscillator at the same forcing frequencies, $\omega_f/\omega_n \approx 0.92$ and 1.08. We base this speculation on the fact that the Poincaré maps for f_f far from f_n (including $f_f/f_n \approx 0.92$ and 1.08) are qualitatively different from those for f_f close to f_n. We will discuss this difference in § 3.2.2 (f_f far from f_n) but for now it suggests that lock-in without frequency pulling occurs via a different type of bifurcation than does lock-in with frequency pulling. Before

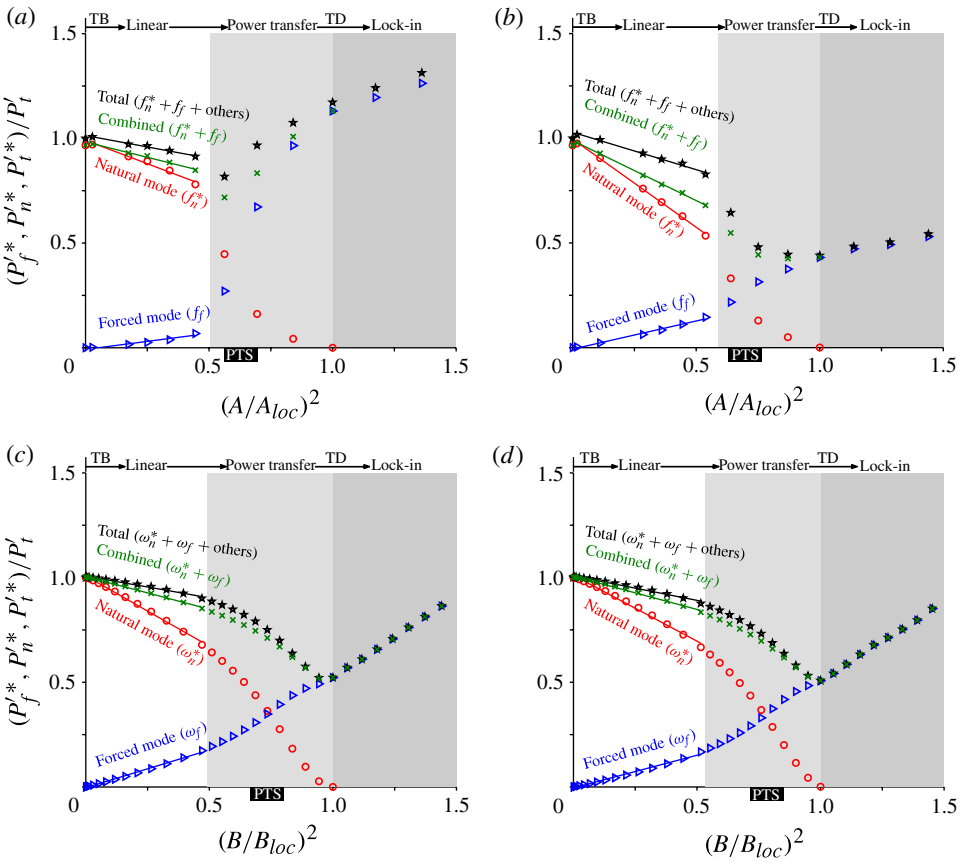

FIGURE 9. (Colour online) Spectral power of oscillations as a function of the forcing power for (*a,b*) the jet and (*c,d*) the VDP oscillator. Two forcing frequencies are considered, both far from the natural frequency: $f_f/f_n = \omega_f/\omega_n \approx 0.88$ (*a,c*) and 1.12 (*b,d*). The linear regime is entered at $(A/A_{loc})^2 = (B/B_{loc})^2 = 0$ via a torus-birth (TB) bifurcation. The lock-in regime is entered at $(A/A_{loc})^2 = (B/B_{loc})^2 = 1$ via a torus-death (TD) bifurcation without frequency pulling. The forcing power at which $P_f'^*$ ($\triangleright$) overtakes $P_n'^*$ ($\circ$) is that at which the peak torus size (PTS) occurs. The combined power, $P_n'^* + P_f'^*$, is denoted by $\times$, and $P_t'^*$ by $\star$.

proceeding, we note that forcing the jet at $f_f/f_n \approx 0.84$ gives rise to a complicated (possibly chaotic) response in which we cannot find a definitive bifurcation to lock-in. We speculate that this may be due to an overlap of the 1:1 Arnol'd tongue (which is asymmetric towards $f_f/f_n < 1$, § 3.2.3) with its adjacent higher-order tongues. Because we consider only 1:1 lock-in in this paper, however, we cannot confirm this speculation and therefore exclude this particular data set from figure 8(*a*).

3.2.2. *Leading up to lock-in: f_f far from f_n* ($|1 - f_f/f_n| \gtrsim 0.07$)

Without frequency pulling, lock-in occurs through a decrease in the power of the natural mode, $P_n'^*$, and an increase in the power of the forced mode, $P_f'^*$. This process, known as asynchronous quenching (Dewan 1972), is shown in figure 9 alongside the total power, $P_t'^*$, for two forcing frequencies, both far from the natural frequency: $f_f/f_n = \omega_f/\omega_n \approx 0.88$ and 1.12. The corresponding time traces, PSDs and

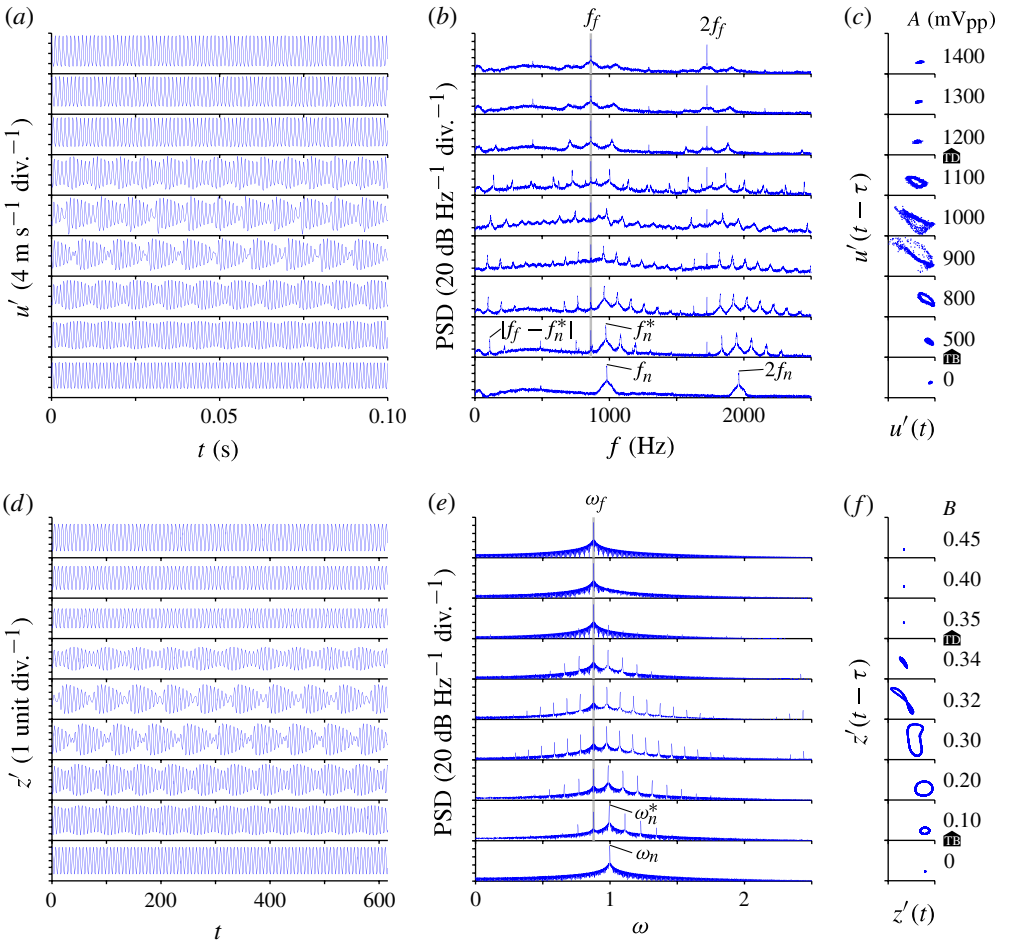

FIGURE 10. (Colour online) Forced response of (*a–c*) the jet and (*d–f*) the VDP oscillator for a forcing frequency far below the natural frequency: $f_f/f_n = \omega_f/\omega_n \approx 0.88$. For both systems, the (*a,d*) time trace, (*b,e*) PSD and (*c,f*) Poincaré map are shown for eight forcing amplitudes and for the unforced case. The transition from periodicity to quasiperiodicity occurs via a torus-birth bifurcation: see the arrows labelled TB ($A = 0 \to 500\ \mathrm{mV_{pp}}$; $B = 0 \to 0.10$). The transition from quasiperiodicity to lock-in occurs via a torus-death bifurcation without frequency pulling: see the arrows labelled TD ($A = 1100 \to A_{loc} = 1200\ \mathrm{mV_{pp}}$; $B = 0.34 \to B_{loc} = 0.35$).

Poincaré maps are shown in figures 10 and 11. All three powers ($P_n'^*$, $P_f'^*$, $P_t'^*$) are normalized by the total power of the unforced oscillations (P_t', without an asterisk) and shown as a function of the forcing power: $(A/A_{loc})^2$ for the jet or $(B/B_{loc})^2$ for the VDP oscillator. The modal power is found by integrating the PSD around each mode, a procedure equivalent to bandpass filtering around each frequency. The total power is found by integrating the PSD across its full bandwidth, and the result is checked to be equal (within 0.2 %) to the mean squared fluctuation, in accordance with Parseval's theorem. In both the jet and the VDP oscillator, three regimes can be identified:

(i) In the linear regime ($0 \leqslant (A/A_{loc})^2 = (B/B_{loc})^2 \lesssim 0.5$), which is quasiperiodic and is entered via a torus-birth bifurcation, $P_f'^*$ increases linearly as $P_n'^*$ decreases

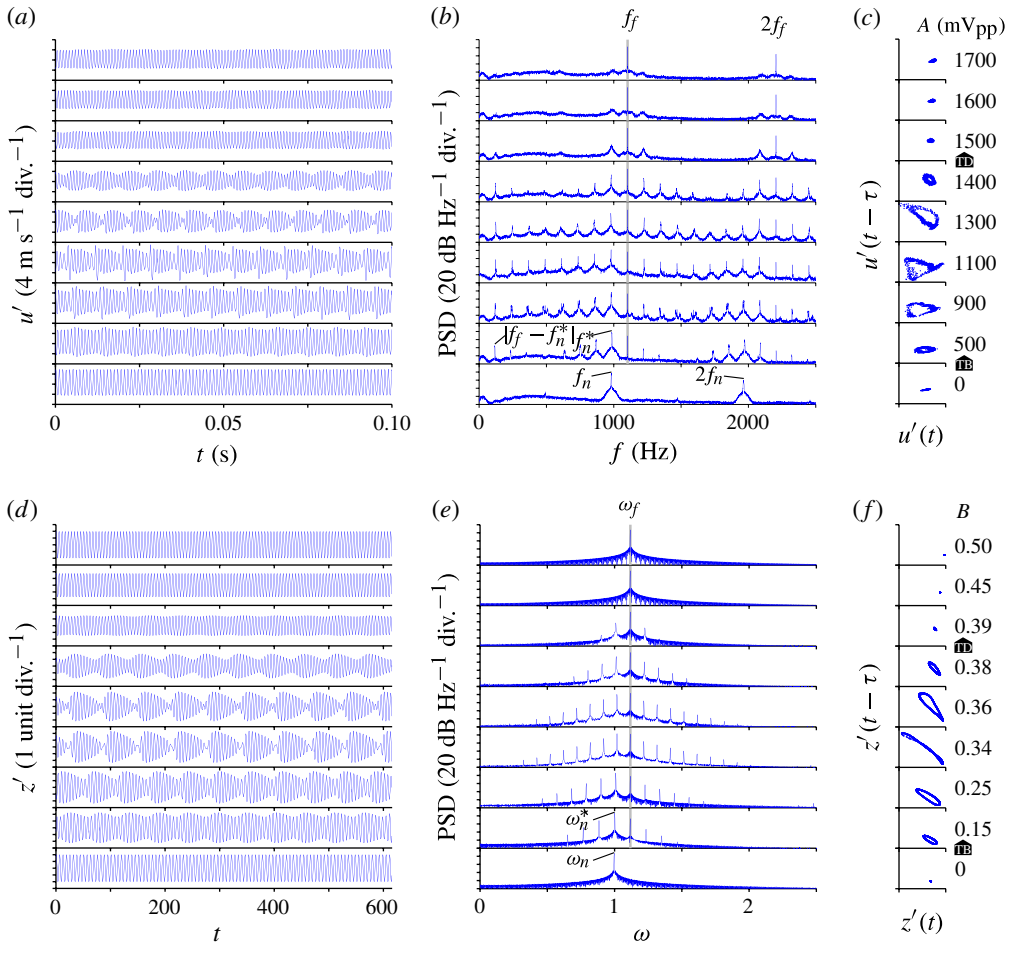

FIGURE 11. (Colour online) Forced response of (*a–c*) the jet and (*d–f*) the VDP oscillator for a forcing frequency far above the natural frequency: $f_f/f_n = \omega_f/\omega_n \approx 1.12$. For both systems, the (*a,d*) time trace, (*b,e*) PSD and (*c,f*) Poincaré map are shown for eight forcing amplitudes and for the unforced case. The transition from periodicity to quasiperiodicity occurs via a torus-birth bifurcation: see the arrows labelled TB ($A = 0 \rightarrow 500$ mV$_{pp}$; $B = 0 \rightarrow 0.15$). The transition from quasiperiodicity to lock-in occurs via a torus-death bifurcation without frequency pulling: see the arrows labelled TD ($A = 1400 \rightarrow A_{loc} = 1500$ mV$_{pp}$; $B = 0.38 \rightarrow B_{loc} = 0.39$).

linearly. This indicates that, with each increment in forcing power (at f_f or ω_f), a constant proportion of it is supplied to the forced mode, while a different constant proportion of it is removed from the natural mode. The fact that the natural mode is affected at all suggests that nonlinear interactions occur even though the forced mode is still linear: $P_f'^* \propto (A/A_{loc})^2$ or $P_f'^* \propto (B/B_{loc})^2$. The linear increase in $P_f'^*$ has been observed by Sreenivasan *et al.* (1989) and Kyle & Sreenivasan (1993) in both self-excited and convectively unstable jets. The linear decrease in $P_n'^*$, however, has not, to our knowledge, been reported before, although it has been observed by Bellows, Hreiz & Lieuwen (2008) in premixed flames that are self-excited by thermoacoustic, not hydrodynamic, resonance. Its physical

mechanisms must be nonlinear and could act by impairing the natural mode's ability to extract power from the baseflow, by increasing dissipation, and/or by transferring power from the natural mode to its sidebands. Nevertheless, because $P_n'^*$ decreases more strongly than $P_f'^*$ increases, their combined power, $P_n'^* + P_f'^*$, also decreases (linearly). The difference between this combined power and $P_t'^*$ is the power contained in the other components. This residual power increases slightly with the forcing power, causing $P_t'^*$ to decrease (linearly) at a slightly lower rate than the combined power.

(ii) In the power transfer regime ($0.5 \lesssim (A/A_{loc})^2 = (B/B_{loc})^2 \leqslant 1$), which is still quasiperiodic, $P_f'^*$ increases nonlinearly as $P_n'^*$ decreases nonlinearly. This coincident departure from linearity suggests the activation of some mechanism that facilitates the transfer of power from the natural mode to the forced mode. This transfer, however, is not completely efficient as only a fraction of the power lost by the natural mode is gained by the forced mode. The rest is dissipated, contributing to the decrease in $P_t'^*$. In the jet (figure 9*a,b*), this decrease is large at $f_f/f_n \approx 1.12$ but small at $f_f/f_n \approx 0.88$. This is because, at $f_f/f_n \approx 0.88$, more power remains in the natural mode from the previous (linear) regime for subsequent transfer to the forced mode in this regime. In the VDP oscillator (figure 9*c,d*), however, this asymmetry about the natural frequency is absent: $P_t'^*$ decreases to equally low values at both forcing frequencies. In both systems, $P_f'^*$ overtakes $P_n'^*$ at a certain forcing power, indicating a swap of the dominant mode. This swap can be seen in the Poincaré map as a peak in the cross-sectional size of the torus attractor: figure 10 ($A = 900$ mV$_{pp}$; $B = 0.30$) and figure 11 ($A = 1100$ mV$_{pp}$; $B = 0.34$). With further increases in forcing power, the transfer rate from $P_n'^*$ to $P_f'^*$ decreases because $P_n'^* \to 0$, causing $P_f'^*$ to saturate. This is a gradual process, accompanied by a similarly gradual shrinkage of the torus attractor: figure 10 ($A = 1000 \to 1200$ mV$_{pp}$; $B = 0.32 \to 0.35$) and figure 11 ($A = 1300 \to 1500$ mV$_{pp}$; $B = 0.36 \to 0.39$). This gradual approach to lock-in is in stark contrast to the abrupt approach seen in cases with frequency pulling (figures 6 and 7: f_f close to f_n), in which the torus attractor grows and then suddenly becomes resonant at lock-in via a saddle-node bifurcation. In the absence of frequency pulling (figures 10 and 11: f_f far from f_n), the fact that the torus attractor grows, peaks, but then gradually shrinks suggests that lock-in occurs via a different type of bifurcation: a torus-death (inverse Neimark–Sacker) bifurcation. This conclusion, like our earlier one suggesting a saddle-node bifurcation for lock-in with frequency pulling (§ 3.2.1), is consistent with the truncated VDP analysis of Balanov *et al.* (2009, figure 3.12).

(iii) In the lock-in regime ($1 \leqslant (A/A_{loc})^2 = (B/B_{loc})^2 \leqslant 1.5$), $P_t'^*$ is determined mostly by $P_f'^*$ because $P_n'^* \approx 0$ and the other components are weak. In the jet, the asymmetry in $P_t'^*$ about $f_f/f_n = 1$ is still present: $P_t'^*$ can be greater ($f_f/f_n \approx 0.88$) or less ($f_f/f_n \approx 1.12$) than P_t'. In the VDP oscillator, the same asymmetry is again absent: $P_t'^*$ reaches a minimum at the onset of lock-in, $(B/B_{loc})^2 = 1$, whose value is always less than P_t' regardless of whether $\omega_f/\omega_n > 1$ or $\omega_f/\omega_n < 1$.

In summary, we have shown that a self-excited jet responds to forcing in a way that is more complicated than that which is expected from the hydrodynamics literature. When forced at increasing amplitudes, the jet undergoes a sequence of two nonlinear transitions. The first transition, which occurs when A initially increases from zero, is from periodicity to $\mathbb{T}^2$ quasiperiodicity. It always occurs via a torus-birth bifurcation.

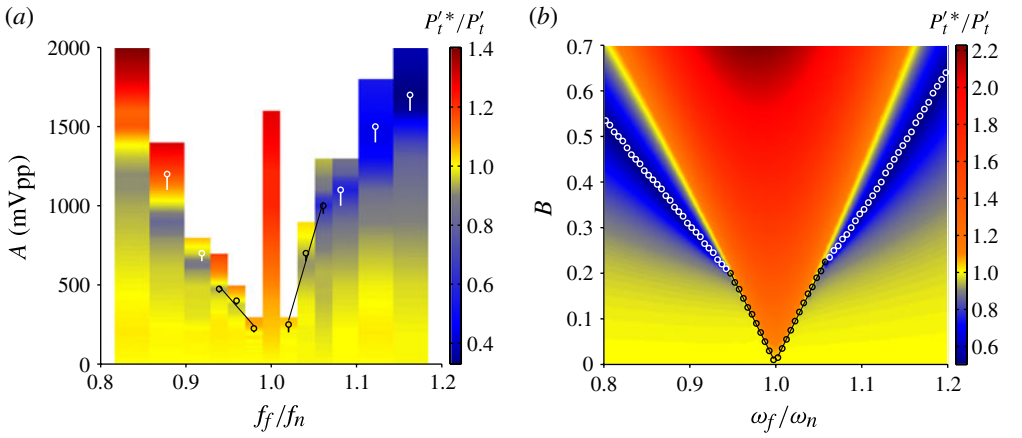

FIGURE 12. (Colour online) Critical forcing amplitude for lock-in (circular markers) shown on contours of the total oscillation power for (*a*) the jet and (*b*) the VDP oscillator. The transition from periodicity to quasiperiodicity occurs at $A = B = 0$ via a torus-birth bifurcation. The transition from quasiperiodicity to lock-in occurs at the circular markers via either a saddle-node bifurcation (black) or a torus-death bifurcation (white). In (*a*) the error bars denote the A increment used just before lock-in.

The second transition, which occurs when A reaches a critical value, is from $\mathbb{T}^2$ quasiperiodicity to 1:1 lock-in. It occurs via either a saddle-node bifurcation with frequency pulling, if f_f and f_n are close together, or a torus-death bifurcation without frequency pulling, but with a gradual suppression of the natural mode, if the two frequencies are far apart. Qualitatively, all of these transitions and bifurcations are accurately reproduced by the forced VDP oscillator. The only feature not reproduced is an asymmetry in $P_t'^*$ about $f_f/f_n = 1$, which we will explore next.

3.2.3. *At lock-in*

In this section, we examine the forced response at lock-in. We start with the relationship between the minimum forcing amplitude required for lock-in, A_{loc} or B_{loc}, and the normalized forcing frequency, f_f/f_n or ω_f/ω_n. This is known as the 1:1 Arnol'd tongue in dynamical systems terminology. It is shown in figure 12 as circular markers, which are coloured black for saddle-node bifurcations and white for torus-death bifurcations. The black diagonal lines on either side of the natural frequency are linear fits to the saddle-node data. As is the case before lock-in (§§ 3.2.1 and 3.2.2), we find striking similarities, but also subtle differences, between the jet and the VDP oscillator:

(i) When forced close to the natural frequency (saddle-node bifurcation), both systems have values of A_{loc} or B_{loc} that increase as the forcing frequency deviates from the natural frequency. This increase is linear, giving rise to a characteristic $\vee$-shaped curve, similar to those reported by Provansal *et al.* (1987), Bellows *et al.* (2008), Davitian *et al.* (2010), Getsinger *et al.* (2012) and Li & Juniper (2013) for other self-excited flows. In the jet (figure 12*a*), there is a new asymmetry about $f_f/f_n = 1$: lock-in occurs more readily for $f_f/f_n < 1$ than it does for $f_f/f_n > 1$. A similar asymmetry has been observed by Getsinger *et al.* (2012) in low-density cross-flowing jets and by Blevins (1985) and Provansal *et al.* (1987) in cylinder

wakes, although an opposite one has been observed by Davitian *et al.* (2010) in equidensity cross-flowing jets and by Li & Juniper (2013) in jet diffusion flames. In the VDP oscillator (figure 12*b*), this asymmetry is also present but is not as strong. According to our supplemental simulations (appendix B), its strength, as measured by the difference in slope of the two black lines, remains relatively constant with increasing ϵ, which suggests that it is not a dominant feature of nonlinearity. Nevertheless, increasing ϵ causes the boundary between saddle-node and torus-death bifurcations to deviate from the natural frequency. For this paper, we specifically chose to use $\epsilon = 0.2$ because this places that boundary at a frequency that matches that found for the jet: $|1 - f_f/f_n| \approx 0.07$.

(ii) When forced far from the natural frequency (torus-death bifurcation), both systems continue to have values of A_{loc} or B_{loc} that increase linearly as the forcing frequency deviates from the natural frequency. However, the slope of this increase changes. For the jet, it decreases for $f_f/f_n > 1$ and increases for $f_f/f_n < 1$. For the VDP oscillator, it decreases for either $\omega_f/\omega_n > 1$ or $\omega_f/\omega_n < 1$.

Also shown in figure 12 are contours of $P_t'^*/P_t'$. For the jet (figure 12*a*), as A increases, this power ratio first decreases from unity and reaches a minimum before or at lock-in (the value of this minimum decreases as f_f/f_n deviates from 1). It then either increases above unity ($f_f/f_n < 1$) or stays below it ($f_f/f_n > 1$), confirming the asymmetry about $f_f/f_n = 1$ that was noticed in figure 9. A similar asymmetry has been observed by Hallberg & Strykowski (2008) in similar low-density jets and by Li & Juniper (2013) in jet diffusion flames. Finally, as A increases for $f_f/f_n = 1$, $P_t'^*/P_t'$ increases from unity and saturates. Except for the asymmetry, these features are also exhibited by the VDP oscillator (figure 12*b*).

In summary, we have shown that a self-excited jet locks in most readily when forced close to f_n, as expected. What was not expected, though, was that the details would depend on whether it is forced above or below f_n. When forced above f_n, the jet is more resistant to lock-in, and its oscillations at lock-in are relatively weak. When forced below f_n, it is less resistant to lock-in, and its oscillations at lock-in are relatively strong. Qualitatively, all of these dynamics are accurately reproduced by the forced VDP oscillator, with the only exception being the asymmetry in $P_t'^*$ about $f_f/f_n = 1$.

3.3. *Other low-dimensional models*

Before concluding this paper, we note that other low-dimensional models can give similar results. One example is the Landau–Stuart model, which has been used by many researchers to study the supercritical Hopf bifurcation to a global mode (see the review by Huerre & Monkewitz 1990). With external sinusoidal forcing, it has the form:

$$\frac{\mathrm{d}\hat{u}}{\mathrm{d}t} = \hat{\alpha}\hat{u} - \hat{\beta}|\hat{u}|^2\hat{u} + F\mathrm{e}^{\mathrm{i}\omega_f t}, \tag{3.1}$$

where complex quantities are denoted by a hat symbol. For example, $\hat{u}$ is the complex velocity fluctuation, defined as $\hat{u}(t) = \sigma(t)\mathrm{e}^{\mathrm{i}\psi(t)}$, and $\hat{\alpha}$ and $\hat{\beta}$ are the complex Landau–Stuart constants, which are usually determined from experiments. The forcing has an amplitude of F and an angular frequency of ω_f. To solve (3.1), we follow Olinger (1993) by separating it into real and imaginary parts, thus creating a

low-dimensional dissipative system of ordinary differential equations:

$$\frac{\mathrm{d}\sigma}{\mathrm{d}t} = \omega_0(\alpha_r - \beta_r\sigma^2)\sigma + F\cos(\omega_f t - \psi), \tag{3.2}$$

$$\frac{\mathrm{d}\psi}{\mathrm{d}t} = \omega_0(\alpha_\mathrm{i} - \beta_\mathrm{i}\sigma^2) + \frac{F}{\sigma}\sin(\omega_f t - \psi), \tag{3.3}$$

where subscripts r and i denote the real and imaginary parts, respectively. These equations are similar to those of Provansal *et al.* (1987) except that β_i is retained in order to permit non-isochronous oscillations, i.e. oscillations whose frequency depends on the saturated amplitude. As with the VDP oscillator (§ 2.2), we leave ω_0 at 1 but note that this value is not necessarily equal to the natural angular frequency of the actual nonlinear oscillations, ω_n. We solve (3.2) and (3.3) numerically using a multistep variable-order algorithm (Shampine & Reichelt 1997), with Landau–Stuart constants from the cylinder-wake experiments of Sreenivasan, Strykowski & Olinger (1987). We do this for a range of forcing frequencies, but show only two representative values: one close to the natural frequency ($\omega_f/\omega_n \approx 1.04$) in figure 13(*a–c*), which can be compared with figure 6, and one far from it ($\omega_f/\omega_n \approx 1.30$) in figure 13(*d–f*), which can be compared with figure 11. This comparison shows that the forced Landau–Stuart model can qualitatively reproduce most of the transitions, bifurcations and dynamics exhibited by the forced low-density jet and the forced VDP oscillator, including the two different types of bifurcations to lock-in. This agreement is not surprising because, as Albarède & Monkewitz (1992) and Olinger (1993) noted, most suitable temporal models (including the VDP oscillator) can be simplified to the generic Landau–Stuart model near the onset of global instability, in the weakly nonlinear regime.

4. Conclusions

Hydrodynamically self-excited jets are known to lock into strong external forcing, but their dynamics before lock-in and the specific bifurcations through which they lock in have not previously been studied in detail. In this experimental study, we have applied open-loop time-periodic acoustic forcing to a low-density jet that is self-excited at a discrete natural frequency. We applied the forcing around this frequency, at varying amplitudes, and measured the response leading up to lock-in. We then modelled the system as a forced VDP oscillator in order to better understand its underlying dynamics.

Our results show that a self-excited jet responds to forcing in a way that is more complicated than that which is expected from the hydrodynamics literature. When forced at increasing amplitudes, the jet undergoes a sequence of two nonlinear transitions: (i) from periodicity to $\mathbb{T}^2$ quasiperiodicity via a torus-birth bifurcation; and then (ii) from $\mathbb{T}^2$ quasiperiodicity to 1:1 lock-in via either a saddle-node bifurcation with frequency pulling, if f_f and f_n are close together, or a torus-death bifurcation without frequency pulling, but with a gradual suppression of the natural mode, if the two frequencies are far apart. The jet locks in most readily when forced close to f_n, but the details contain two asymmetries about $f_f/f_n = 1$: (i) the critical forcing amplitude for lock-in is lower and (ii) the total oscillation power is higher for $f_f/f_n < 1$ than for $f_f/f_n > 1$.

Except for the second asymmetry, all of these transitions, bifurcations and dynamics are accurately reproduced by the forced VDP oscillator. This shows that this

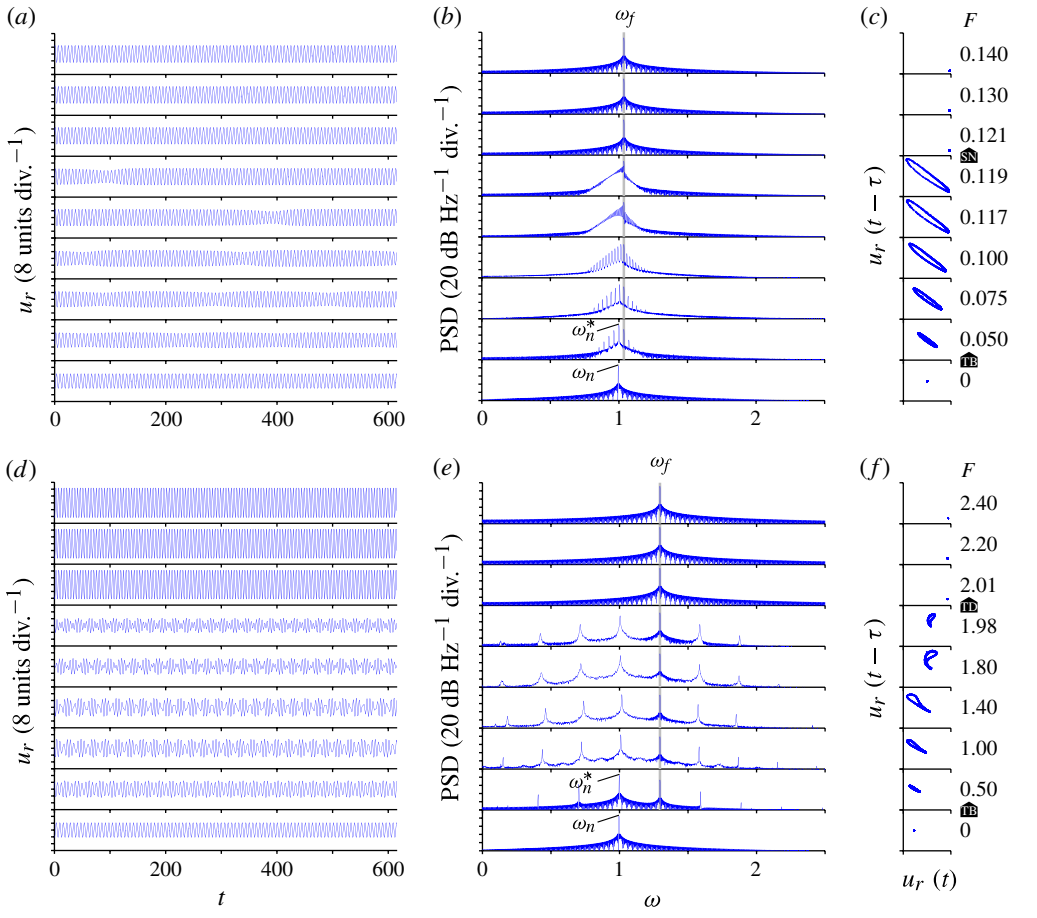

FIGURE 13. (Colour online) Forced response of the Landau–Stuart model for two different forcing frequencies: one close to the natural frequency (*a–c*: $\omega_f/\omega_n \approx 1.04$) and one far from it (*d–f*: $\omega_f/\omega_n \approx 1.30$). For both frequencies, the (*a,d*) time trace, (*b,e*) PSD and (*c,f*) Poincaré map of the real part of $\hat{u}$ are shown for eight forcing amplitudes and for the unforced case. The transition from periodicity to quasiperiodicity occurs via a torus-birth bifurcation: see the arrows labelled TB (*a–c*: $F = 0 \rightarrow 0.050$; *d–f*: $F = 0 \rightarrow 0.50$). The transition from quasiperiodicity to lock-in occurs via either a saddle-node bifurcation with frequency pulling (see arrow labelled SN in *a–c*: $F = 0.119 \rightarrow F_{loc} = 0.121$), if ω_f and ω_n are close together, or a torus-death bifurcation without frequency pulling, but with a suppression of the natural mode (see arrow labelled TD in *d–f*: $F = 1.98 \rightarrow F_{loc} = 2.01$), if the two frequencies are far apart.

forced self-excited jet with infinite DOFs can be modelled reasonably well as a nonlinear dynamical system with just three DOFs. This result is consistent with previous suggestions that open self-excited flows belong to a generic class of dissipative dynamical systems that is amenable to low-dimensional modelling. It raises the possibility that other, more industrially relevant, self-excited flows— such as multiphase, combusting, compressible and/or turbulent jets and wakes— can be similarly modelled. This would not only strengthen the universality of such flows,

but would also provide a predictive capability that could be useful to engineers from various fields.

In the development of gas turbines and rocket engines, for example, a recurring problem is thermoacoustic instability (Zinn & Lieuwen 2005). This occurs when heat-release and pressure oscillations in a combustor interact such that thermal energy is fed into the acoustic waves. If these waves are insufficiently damped, they can grow to dangerously high amplitudes. In experiments on a flame with an intrinsic hydrodynamic instability, Chakravarthy *et al.* (2007) showed that they grow to particularly high amplitudes when the heat-release oscillations lock into the acoustic oscillations. In many fuel injectors, the heat-release oscillations are caused by the hydrodynamic oscillations of the flame. Several mechanisms are possible for this, but most rely on the development of coherent flow structures (e.g. large-scale vortices). These structures can (i) entrain pockets of reactants and transport them to regions hot enough for delayed ignition (Rogers & Marble 1956); (ii) impinge on the flame and cause its surface area, and hence its heat release, to vary in time (Balachandran *et al.* 2005); and/or (iii) break down into fine-scale turbulence to aid molecular mixing of the air and fuel, thereby causing sudden increases in heat release (Schadow & Gutmark 1992). For the suppression of thermoacoustic instability, therefore, it would be useful to be able to predict how the hydrodynamic oscillations of a flame interact with the acoustic oscillations of its combustor.

Our low-dimensional modelling of the forced low-density jet is a first step towards achieving this predictive capability. Our next step is to apply the same modelling to a simple self-excited flame: a jet diffusion flame. Our preliminary findings indicate that, like the low-density jet, this flame can exhibit several different nonlinear states, such as periodicity, quasiperiodicity and lock-in, depending on the forcing parameters (Li & Juniper 2013). However, we have yet to confirm whether it also transitions between those states via the same bifurcations as those seen in the forced VDP oscillator. Nevertheless, the jet diffusion flame is not widely used in gas turbines because of its low combustion efficiency and high pollutant emissions (e.g. nitrogen oxides and soot). We will therefore perform similar experiments and modelling on a more relevant configuration: a premixed or partially premixed flame stabilized behind a bluff-body within an acoustic duct. This system will be susceptible not only to the self-excited vortex shedding that develops in the near-wake region (Anderson, Hertzberg & Mahalingam 1996), but also to thermoacoustic oscillations. These occur when acoustic perturbations impinge on the flame base and cause heat-release perturbations some time later, e.g. by perturbing the surface area and stretch of the flame as they travel down its body. If the heat release increases at moments of higher pressure and decreases at moments of lower pressure, then this mechanism can cause the acoustic energy to increase over a cycle. This mechanism and the hydrodynamic mechanism can exist independently but, as Chakravarthy *et al.* (2007) showed, they can also interact with each other if their frequencies are similar. Following on from the approach in this paper, we will model this interacting system as two coupled oscillators. The stability of this system will depend on the way in which the individual oscillators force each other. This approach is analogous to that which is often used to study vortex-induced vibration, in which the hydrodynamics is represented by one oscillator and the structural dynamics by another. Regardless of the specific application, though, the accurate representation of an infinite-dimensional forced self-excited flow by a low-dimensional ordinary differential equation remains one of the most crucial steps in the modelling process, for which the results in this paper will be valuable.

Acknowledgements

We would like to thank the Bill & Melinda Gates Foundation and Trinity College Cambridge for their financial support. We would also like to thank D. Durox from École centrale de Paris for loaning us his injector.

Appendix A. Correlation dimension

The correlation dimension is a topological measure of the self-similarity of an attractor. In other words, it is a measure of the number of active DOFs in a dynamical system. Compared with other fractal dimensions (for a full list, see Kantz & Schreiber 2003), it is relatively easy to calculate, even for an attractor that has been reconstructed from an experimental time series of finite duration. For this reason, it is often used to diagnose the underlying dynamics. Its value is zero for a steady flow (fixed point), one for a periodic limit cycle (closed trajectory), two for a quasiperiodic oscillation with two incommensurate modes (torus surface), fractional for a chaotic motion (self-similar fractal) and infinite for a purely stochastic process (random noise).

To calculate the correlation dimension, we use the algorithm of Grassberger & Procaccia (1983), as did Gotoda & Ueda (2002) and Lieuwen (2002). The details can be found in the original paper, as well as in the book chapter by Henry, Lovell & Camacho (2000). The algorithm relies on one key assumption: the probability that two points on an attractor occupy the same R-sized cell is approximately the same as the probability that they are separated by a distance less than or equal to R. Mathematically, this is implemented by considering an m-dimensional hypersphere centred around a point on the attractor in Euclidean space $\mathbb{R}^m$, where m is the embedding dimension, as defined in § 2.3. The number of neighbouring points enclosed by the hypersphere is estimated as a function of its radius R with the correlation sum:

$$C(m,R) \approx \frac{\sum_{i=1,j\neq i}^{n} H(R - \|\boldsymbol{\xi}(t_i) - \boldsymbol{\xi}(t_j)\|)}{(n/2)(n-1)}, \tag{A 1}$$

where n is the number of data points in each element u' of the time-delayed vector $\boldsymbol{\xi}(t)$, as defined in (2.2). The approximation in (A 1) becomes exact in the limit $n \to \infty$. The Heaviside step function is defined as

$$H(s) = \begin{cases} 1 & \text{for } s \geqslant 0 \\ 0 & \text{for } s < 0, \end{cases} \tag{A 2}$$

which means that, as the hypersphere moves around the attractor and grows, $C(m,R)$ increments every time R is greater than or equal to the Euclidean distance between the vectors $\boldsymbol{\xi}(t_i)$ and $\boldsymbol{\xi}(t_j)$. This distance is defined as the following norm:

$$\|\boldsymbol{\xi}(t_i) - \boldsymbol{\xi}(t_j)\| = \sqrt{\sum_{k=0}^{m-1} (u'(t_i - k\tau) - u'(t_j - k\tau))^2}. \tag{A 3}$$

The number of data points in the hypersphere scales with R according to a power law but the exponent depends on R itself. This is because the dimension of any geometric object depends on the magnification at which it is viewed. A ball of string, for example, appears as a zero-dimensional point from afar, as a three-dimensional

solid from a few metres, as a one-dimensional intertwined string from a few centimetres, and as a three-dimensional intertwined string of solid fibres from under a microscope. An attractor in phase space, similarly, appears as a zero-dimensional point at large scales (large R) but as a high-dimensional object at small scales (small R). The increased dimensionality at small scales is due to the increased influence of background noise, which imparts a degree of stochasticity and thus activates additional DOFs. If the scale of such noise is R_N, the correlation sum typically increases as follows:

$$C(m,R) \propto \begin{cases} R^m & \text{for } R < R_N \\ R^D & \text{for } R > R_N, \end{cases} \tag{A 4}$$

where, for many physical systems, the exponent D is constant over an appreciable, but finite, range of R larger than R_N. This range is known as the self-similar scaling region, and the value of D within it is an estimate of the correlation dimension, D_2. In this paper, we estimate D_2 by plotting $\log C(m,R)$ versus $\log R$ and then finding the value to which the slope of the linear region converges as m increases. For reliable convergence, we use up to $m = 7$, which is sufficiently larger than the largest expected attractor dimension. If the signal were from a purely stochastic process, however, then even a very large m would not lead to convergence, because the actual attractor would have infinitely many active DOFs and hence infinitely many dimensions.

In figure 14, we show results from a D_2 calculation performed on the low-density jet at the conditions of figure 6. We consider three forcing amplitudes:

(i) For no forcing ($A = 0\ \mathrm{mV_{pp}}$), $D_2 \approx 1$ over an order of magnitude of scales ($0.04 \lesssim R/R_{max} \lesssim 0.4$), indicating a periodic limit cycle with one DOF. Beyond either end of this scaling region, the local slope of $C(m,R)$ does not converge, indicating an absence of self-similarity at extreme scales. According to Kantz & Schreiber (2003), at very small scales, the dynamics are dominated by noise. Noise tends to randomly displace the phase trajectory away from its intended path, thus activating additional DOFs and causing the local slope of $C(m,R)$ to increase with m. At very large scales, self-similarity is disrupted by the finite scale of the attractor, which acts as a macroscopic cutoff filter.

(ii) For weak forcing ($A = 300\ \mathrm{mV_{pp}}$), $D_2 \approx 2$ over a range of intermediate scales ($0.03 \lesssim R/R_{max} \lesssim 0.06$), indicating a quasiperiodic oscillation with two incommensurate modes. This primary scaling region is followed by a secondary scaling region at slightly larger scales ($0.1 \lesssim R/R_{max} \lesssim 0.4$) for which $D_2 \approx 1$. These two scaling regions coexist because, at the inception of quasiperiodicity (i.e. just after a torus-birth bifurcation), the minor radius of the torus attractor is still much smaller than the major radius. In other words, there is a distinct separation of scales. According to Theiler (1986), the most representative value of D_2 for systems with multiple scaling regions is that which is found at the smallest scales. This is because D_2 is defined strictly for $R \to 0$, although, in practice, noise and discretization errors prevent this limit from being reached. We therefore classify this attractor as a torus attractor with two DOFs ($\mathbb{T}^2$).

(iii) For strong forcing ($A = 700\ \mathrm{mV_{pp}}$), $D_2 \approx 1$ over an order of magnitude of scales ($0.04 \lesssim R/R_{max} \lesssim 0.4$), indicating another periodic limit cycle with one DOF. Unlike the original (unforced) limit cycle, however, this one is locked into the forcing.

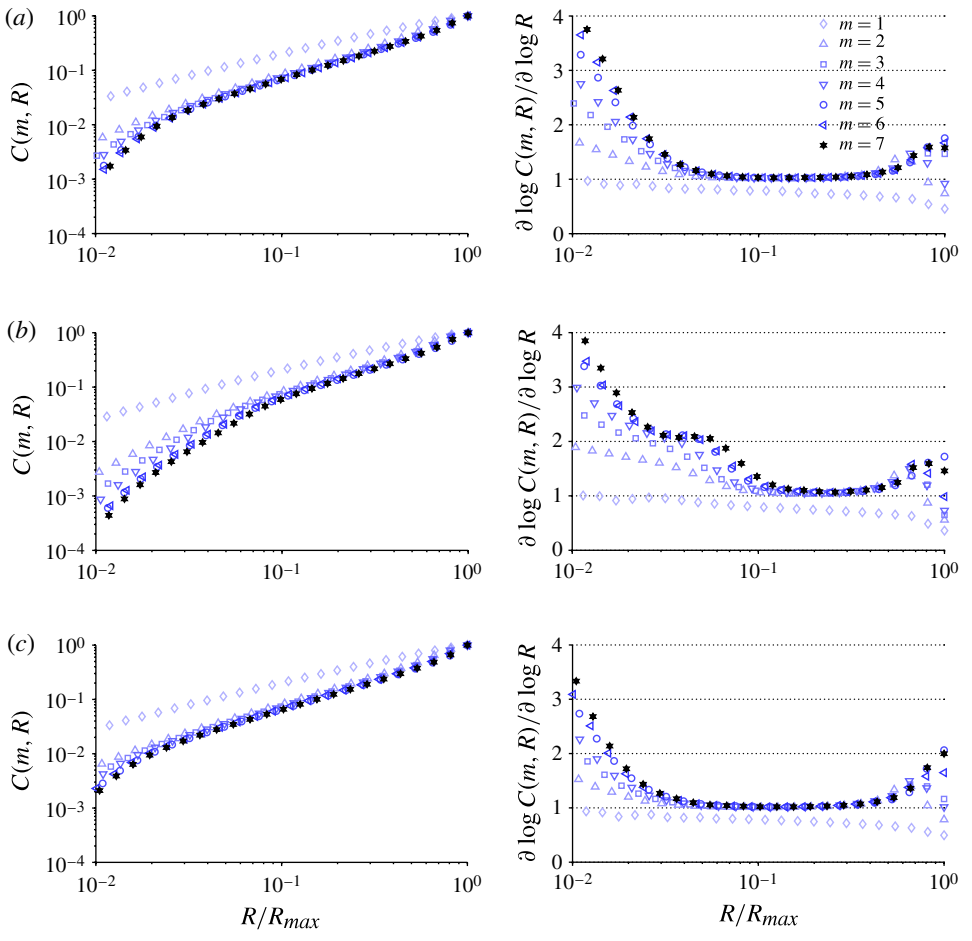

FIGURE 14. (Colour online) Correlation sum (left column) and its local slope (right column), both shown as a function of the Euclidean distance, for an embedding dimension up to $m = 7$. The data are for the low-density jet when forced at a frequency slightly above its natural frequency (figure 6): $f_f/f_n \approx 1.04$. Three forcing amplitudes are considered, giving a range of nonlinear dynamics: (*a*) forced lock-in with one DOF, $A = 700\ \mathrm{mV_{pp}}$; (*b*) forced quasiperiodicity with two DOFs, $A = 300\ \mathrm{mV_{pp}}$; and (*c*) unforced periodicity with one DOF, $A = 0\ \mathrm{mV_{pp}}$.

These results are for a saddle-node bifurcation to lock-in (§ 3.2.1: f_f close to f_n) but are also typical of those for a torus-death bifurcation to lock-in (§ 3.2.2: f_f far from f_n). This shows that, although the specific type of bifurcation to lock-in depends on f_f relative to f_n, the number of active DOFs in the system does not.

Appendix B. Forced VDP oscillator with stronger nonlinearity

We also examine the forced VDP oscillator (2.1) for values of its feedback parameter higher than $\epsilon = 0.2$, the value used so far in this paper. In figure 15, we show the critical forcing amplitude for lock-in (B_{loc}) and the total oscillation power ($P_t'^*/P_t'$) for $\epsilon = 0.4$ and 0.8. This figure can be compared with figure 12(*b*), which is for $\epsilon = 0.2$. We find that increasing ϵ, and thus increasing the degree of

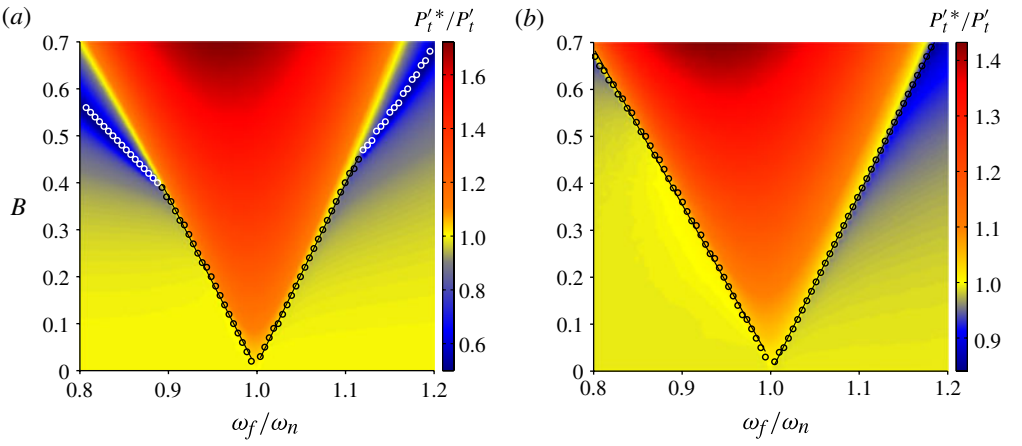

FIGURE 15. (Colour online) Critical forcing amplitude for lock-in (circular markers) shown on contours of the total oscillation power for the forced VDP oscillator at (*a*) $\epsilon = 0.4$ and (*b*) $\epsilon = 0.8$. This figure can be compared with figure 12(*b*), which is for $\epsilon = 0.2$. The transition from periodicity to quasiperiodicity occurs at $B = 0$ via a torus-birth bifurcation. The transition from quasiperiodicity to lock-in occurs at the circular markers via either a saddle-node bifurcation (black) or a torus-death bifurcation (white).

nonlinearity, has two major effects: (i) it causes the boundary between saddle-node and torus-death bifurcations to deviate from the natural frequency, which means that the $\vee$-shaped lock-in curve remains on its initial (saddle-node) slopes for larger deviations from $\omega_f/\omega_n = 1$; and (ii) it causes the total oscillation power to deviate less from $P_t'^*/P_t' = 1$, which means that, over the specific range of $(\omega_f/\omega_n, B)$ shown, the power of the forced oscillations deviates less from that of the unforced oscillations. However, increasing ϵ has only a minor effect on the slopes of the central (saddle-node) portion of the lock-in curve, in which a slight asymmetry towards $\omega_f/\omega_n < 1$ always exists, regardless of the degree of nonlinearity.

REFERENCES

ABARBANEL, H. D. I. 1996 *Analysis of Observed Chaotic Data*. Springer.

ALBARÈDE, P. & MONKEWITZ, P. A. 1992 A model for the formation of oblique shedding and 'chevron' patterns in cylinder wakes. *Phys. Fluids* A **4** (4), 744–756.

ANDERSON, K. R., HERTZBERG, J. & MAHALINGAM, S. 1996 Classification of absolute and convective instabilities in premixed bluff body stabilized flames. *Combust. Sci. Technol.* **112** (1), 257–269.

BAEK, S. J. & SUNG, H. J. 2000 Quasi-periodicity in the wake of a rotationally oscillating cylinder. *J. Fluid Mech.* **408**, 275–300.

BALACHANDRAN, R., AYOOLA, B. O., KAMINSKI, C. F., DOWLING, A. P. & MASTORAKOS, E. 2005 Experimental investigation of the nonlinear response of turbulent premixed flames to imposed inlet velocity oscillations. *Combust. Flame* **143** (1–2), 37–55.

BALANOV, A., JANSON, N., POSTNOV, D. & SOSNOVTSEVA, O. 2009 1:1 forced synchronization of periodic oscillations. In *Synchronization: From Simple to Complex*. chap. 3, Springer.

BARBI, C., FAVIER, D. P., MARESCA, C. A. & TELIONIS, D. P. 1986 Vortex shedding and lock-on of a circular cylinder in oscillatory flow. *J. Fluid Mech.* **170**, 527–544.

BELLOWS, B. D., HREIZ, A. & LIEUWEN, T. 2008 Nonlinear interactions between forced and self-excited acoustic oscillations in premixed combustor. *J. Propul. Power* **24** (3), 628–631.

BLEVINS, R. D. 1985 The effect of sound on vortex shedding from cylinders. *J. Fluid Mech.* **161**, 217–237.

BROZE, G. & HUSSAIN, F. 1994 Nonlinear dynamics of forced transitional jets: periodic and chaotic attractors. *J. Fluid Mech.* **263**, 93–132.

CHAKRAVARTHY, S. R., SHREENIVASAN, O. J., BOEHM, B., DREIZLER, A. & JANICKA, J. 2007 Experimental characterization of onset of acoustic instability in a nonpremixed half-dump combustor. *J. Acoust. Soc. Am.* **122** (1), 120–127.

CHOMAZ, J. M. 2005 Global instabilities in spatially developing flows: non-normality and nonlinearity. *Annu. Rev. Fluid Mech.* **37**, 357–392.

CRAIK, A. D. D. 1988 *Wave Interactions and Fluid Flows*. Cambridge University Press.

DAVITIAN, J., GETSINGER, D., HENDRICKSON, C. & KARAGOZIAN, A. R. 2010 Transition to global instability in transverse-jet shear layers. *J. Fluid Mech.* **661**, 294–315.

DEWAN, E. M. 1972 Harmonic entrainment of van der Pol oscillations: phaselocking and asynchronous quenching. *IEEE Trans. Automat. Control* **17** (5), 655–663.

FACCHINETTI, M. L., DE LANGRE, E. & BIOLLEY, F. 2002 Vortex shedding modelling using diffusive van der Pol oscillators. *C. R. Mec.* **330**, 451–456.

FACCHINETTI, M. L., DE LANGRE, E. & BIOLLEY, F. 2004 Coupling of structure and wake oscillators in vortex-induced vibrations. *J. Fluid Struct.* **19** (2), 123–140.

FAUVE, S. 1998 Pattern forming instabilities. In *Hydrodynamics and Nonlinear Instabilities* (ed. C. Godrèche & P. Manneville). chap. 4, Cambridge University Press.

FRASER, A. M. & SWINNEY, H. L. 1986 Independent coordinates for strange attractors from mutual information. *Phys. Rev.* A **33** (2), 1134–1140.

GASTER, M. 1969 Vortex shedding from slender cones at low Reynolds numbers. *J. Fluid Mech.* **38** (3), 565–576.

GETSINGER, D. R., HENDRICKSON, C. & KARAGOZIAN, A. R. 2012 Shear layer instabilities in low-density transverse jets. *Exp. Fluids* **53** (3), 783–801.

GOTODA, H. & UEDA, T. 2002 Transition from periodic to non-periodic motion of a Bunsen-type premixed flame tip with burner rotation. *Proc. Combust. Inst.* **29** (1), 1503–1509.

GRASSBERGER, P. & PROCACCIA, I. 1983 Characterization of strange attractors. *Phys. Rev. Lett.* **50** (5), 346–349.

GUICKING, D. & HAARS, K. 1991 On the natural frequency of the van der Pol oscillator. *Acustica* **73** (3), 158–161.

HALLBERG, M. P., SRINIVASAN, V., GORSE, P. & STRYKOWSKI, P. J. 2007 Suppression of global modes in low-density axisymmetric jets using coflow. *Phys. Fluids* **19** (1) 014102.

HALLBERG, M. P. & STRYKOWSKI, P. J. 2006 On the universality of global modes in low-density axisymmetric jets. *J. Fluid Mech.* **569**, 493–507.

HALLBERG, M. P. & STRYKOWSKI, P. J. 2008 Open-loop control of fully nonlinear self-excited oscillations. *Phys. Fluids* **20** (4) 041703.

HARTLEN, R. T. & CURRIE, I. G. 1970 Lift-oscillator model of vortex-induced vibration. *J. Engng Mech. ASCE* **96** (5), 577–591.

HENRY, B., LOVELL, N. & CAMACHO, F. 2000 Nonlinear dynamics time series analysis. In *Nonlinear Biomedical Signal Processing: Dynamic Analysis and Modelling* (ed. M. Akay). chap. 1, Wiley–IEEE.

HILBORN, R. C. 2000 *Chaos and Nonlinear Dynamics*, 2nd edn. Oxford University Press.

HO, C. M. & HUERRE, P. 1984 Perturbed free shear layers. *Annu. Rev. Fluid Mech.* **16**, 365–424.

HOLMES, P. J. & RAND, D. A. 1978 Bifurcations of the forced van der Pol oscillator. *Q. Appl. Maths* **35**, 495–509.

HUERRE, P. & MONKEWITZ, P. A. 1990 Local and global instabilities in spatially developing flows. *Annu. Rev. Fluid Mech.* **22**, 473–537.

IWAN, W. D. & BLEVINS, R. D. 1974 A model for vortex induced oscillation of structures. *J. Appl. Mech.* **41** (3), 581–586.

JENDOUBI, S. & STRYKOWSKI, P. J. 1994 Absolute and convective instability of axisymmetric jets with external flow. *Phys. Fluids* **6** (9), 3000–3009.

JOHNSON, A., UDDIN, M. & POLLARD, A. 2005 Calibration of hot-wire probes using non-uniform mean velocity profiles. *Exp. Fluids* **39** (3), 525–532.

JUNIPER, M. P., LI, L. K. B. & NICHOLS, J. W. 2009 Forcing of self-excited round jet diffusion flames. *Proc. Combust. Inst.* **32** (1), 1191–1198.

KANTZ, H. & SCHREIBER, T. 2003 *Nonlinear Time Series Analysis*, 2nd edn. Cambridge University Press.

KARNIADAKIS, G. E. & TRIANTAFYLLOU, G. S. 1989 Frequency selection and asymptotic states in laminar wakes. *J. Fluid Mech.* **199**, 441–469.

KENNEL, M. B., BROWN, R. & ABARBANEL, H. D. I. 1992 Determining embedding dimension for phase-space reconstruction using a geometrical construction. *Phys. Rev.* A **45** (6), 3403–3411.

KOEPKE, M. E. & HARTLEY, D. M. 1991 Experimental verification of periodic pulling in a nonlinear electronic oscillator. *Phys. Rev.* A **44** (10), 6877–6887.

KOOPMANN, G. H. 1967 The vortex wakes of vibrating cylinders at low Reynolds numbers. *J. Fluid Mech.* **28** (3), 501–512.

KUZNETSOV, Y. 2004 *Elements of Applied Bifurcation Theory*, 3rd edn. Springer.

KYLE, D. M. & SREENIVASAN, K. R. 1993 The instability and breakdown of a round variable-density jet. *J. Fluid Mech.* **249**, 619–664.

LESSHAFFT, L., HUERRE, P., SAGAUT, P. & TERRACOL, M. 2006 Nonlinear global modes in hot jets. *J. Fluid Mech.* **554**, 393–409.

LESSHAFFT, L. & HUERRE, P. 2007 Linear impulse response in hot round jets. *Phys. Fluids* **19** (2), 024102.

LI, L. K. B. 2011 Forcing of globally unstable jets and flames. PhD thesis, University of Cambridge, Department of Engineering.

LI, L. K. B. & JUNIPER, M. P. 2013 Lock-in and quasiperiodicity in hydrodynamically self-excited flames: experiments and modelling. *Proc. Combust. Inst.* **34** (1), 947–954.

LIEUWEN, T. C. 2002 Experimental investigation of limit-cycle oscillations in an unstable gas turbine combustor. *J. Propul. Power* **18** (1), 61–67.

MANNEVILLE, P. 2010 *Instabilities, Chaos and Turbulence*, 2nd edn. Imperial College Press.

MEHTA, R. D. & BRADSHAW, P. 1979 Design rules for small low speed wind tunnels. *Aeronaut. J.* **83** (827), 443–449.

MONKEWITZ, P. A., BECHERT, D. W., BARSIKOW, B. & LEHMANN, B. 1990 Self-excited oscillations and mixing in a heated round jet. *J. Fluid Mech.* **213**, 611–639.

MONKEWITZ, P. A., HUERRE, P. & CHOMAZ, J. M. 1993 Global linear stability analysis of weakly non-parallel shear flows. *J. Fluid Mech.* **251**, 1–20.

MULLIN, T. & PRICE, T. J. 1989 An experimental observation of chaos arising from the interaction of steady and time-dependent flows. *Nature* **340**, 294–296.

NAYFEH, A. H. & BALACHANDRAN, B. 2004 *Applied Nonlinear Dynamics: Analytical, Computational, and Experimental Methods*. Wiley–VCH.

NICHOLS, J. W., CHOMAZ, J. M. & SCHMID, P. J. 2007 Secondary instability in variable-density round jets. In *Advances in Turbulence XI: Proceedings of the 11th EUROMECH European Turbulence Conference* (ed. J. M. L. M. Palma & A. Silva Lopes). Springer Series in Physics, vol. 117. pp. 32–34. Springer.

NOACK, B. R., OHLE, F. & ECKELMANN, H. 1991 On cell formation in vortex streets. *J. Fluid Mech.* **227**, 293–308.

OLINGER, D. J. 1992 Lock-in states in the dripping mode of the capillary jet. *Exp. Fluids* **15** (2), 155–158.

OLINGER, D. J. 1993 A low-dimensional model for chaos in open fluid flows. *Phys. Fluids* **5** (8), 1947–1951.

VAN DER POL, B. 1926 On relaxation oscillations. *Phil. Mag.* **2**, 978–992.

VAN DER POL, B. & VAN DER MARK, J. 1927 Frequency demultiplication. *Nature* **120**, 363–364.

PROVANSAL, M., MATHIS, C. & BOYER, L. 1987 Bénard–von Kármán instability: transient and forced regimes. *J. Fluid Mech.* **182**, 1–22.

ROGERS, D. E. & MARBLE, F. E. 1956 A mechanism for high-frequency oscillations in ramjet combustors and afterburners. *Jet Propul.* **26** (6), 456–462.

SCHADOW, K. C. & GUTMARK, E. 1992 Combustion instability related to vortex shedding in dump combustors and their passive control. *Prog. Energ. Combust.* **18** (2), 117–132.

SETTLES, G. S. 2001 *Schlieren and Shadowgraph Techniques: Visualizing Phenomena in Transparent Media*. Springer.

SHAMPINE, L. F. & REICHELT, M. W. 1997 The MATLAB ODE suite. *SIAM J. Sci. Comput.* **18** (1), 1–22.

SMALL, M. 2005 *Applied Nonlinear Time Series Analysis: Applications in Physics, Physiology and Finance*. World Scientific Publishing Company.

SREENIVASAN, K. R., RAGHU, S. & KYLE, D. 1989 Absolute instability in variable density round jets. *Exp. Fluids* **7** (5), 309–317.

SREENIVASAN, K. R., STRYKOWSKI, P. J. & OLINGER, D. J. 1987 Hopf bifurcation, Landau equation, and vortex shedding behind circular cylinders. In *Forum on Unsteady Flow Separation*, vol. 52. pp. 1–13. ASME.

SRINIVASAN, V., HALLBERG, M. P. & STRYKOWSKI, P. J. 2010 Viscous linear stability of axisymmetric low-density jets: parameters influencing absolute instability. *Phys. Fluids* **22** (2), 024103.

STANSBY, P. K. 1976 The locking-on of vortex shedding due to the cross-stream vibration of circular cylinders in uniform and shear flows. *J. Fluid Mech.* **74** (4), 641–665.

STROGATZ, S. H. 1994 *Nonlinear Dynamics and Chaos*. Perseus Books.

STUDENT, 1908 The probable error of a mean. *Biometrika* **6** (1), 1–25.

SUBBARAO, E. R. & CANTWELL, B. J. 1992 Investigation of a co-flowing buoyant jet: experiments on the effect of Reynolds number and Richardson number. *J. Fluid Mech.* **245**, 69–90.

TAKENS, F. 1981 Detecting strange attractors in turbulence. In *Dynamical Systems and Turbulence* (ed. D.A. Rand & L.S. Young). Lecture Notes in Mathematics, vol. 898. pp. 366–381. Springer.

THEILER, J. 1986 Spurious dimension from correlation algorithms applied to limited time-series data. *Phys. Rev. A – Gen. Phys.* **34** (3), 2427–2432.

VAN ATTA, C. W. & GHARIB, M. 1987 Ordered and chaotic vortex streets behind circular cylinders at low Reynolds numbers. *J. Fluid Mech.* **174**, 113–133.

WELCH, P. D. 1967 The use of fast Fourier transform for the estimation of power spectra: a method based on time averaging over short modified periodograms. *IEEE Trans. Audio Electroacoust.* **15**, 70–73.

ZINN, B. T. & LIEUWEN, T. C. 2005 Combustion instabilities: basic concepts. In *Combustion Instabilities in Gas Turbine Engines: Operational Experience, Fundamental Mechanisms, and Modelling* (ed. T.C. Lieuwen & V. Yang). chap. 1, American Institute of Aeronautics and Astronautics.